PARTICLE RETENTION CHARACTERISTICS IN AN INTERSTITIAL REGIME UNDER CYCLIC FLOW LOADING

By

CHENG-SHENG KU

Bachelor of Science

National Taiwan University

Taipei, Taiwan

1986

Submitted to the Faculty of the
Graduate College of the
Oklahoma State University
in partial fulfillment of
the requirements for
the Degree of
MASTER OF SCIENCE
December, 1991

PARTICLE RETENTION CHARACTERISTICS IN

AN INTERSTITIAL REGIME UNDER

CYCLIC FLOW LOADING

Thesis Approved:

Thesis Advisor

Dean of the Graduate College

ACKNOWLEDGMENTS

The author would like to express his sincere appreciation and thanks to many people who encourage his graduate program.

A special note of appreciation is extended to the principal advisor, Dr. I. T. Hong, for his guidance, patience, and encouragement throughout the graduate program.

Many thanks also go to Dr. P. M. Moretti, and Dr. D. G. Lilley for serving the graduate committee. From their advices and suggestions, I obtain many valuable experiences to this study.

I wish to thank to Dr. R. K. Tessmann, Dr. M. Chen, and Dr. Y. C. Shiau for their guidances and advices to this study. Moreover, special gratitude is expressed to Mr. A. Mikle for his support in the test and Mr. H. Mike for checking the grammar of this research.

My sincerest appreciation is expressed to my parents and other family members, without their support, understanding, and encouragement this undertaking would have been impossible.

Most of all, I thank my lovely friend, Hui Ling, for her understanding and encouragement.

TABLE OF CONTENTS

Chapter		Page
I.	INTRODUCTION	1
II.	PREVIEW INVESTIGATION	5
	Introduction	5
	Filtration	5
	Filter Model	12
III.	THEORY DERIVED AND DYNAMIC MODELLING	27
	Introduction	27
	Model Flow Pattern	27
	Forces and Moments of the Model	32
	The Particle Trajectory Equation and Efficiency	33
	Dynamic Flow Model	40
	Simulation Results and Discussions	46
IV.	EXPERIMENTAL VERIFICATION OF THE FILTER MODEL UNDER DYNAMIC FLOW	61
	Introduction	61
	Test Method	62
	Result of Cyclic Test	68
	Discussion of Results	68
V.	CONCLUSIONS AND RECOMMENDATIONS	79
	Conclusions	79
	Recommendations	81
BIBLIOGRAPHY		83

LIST OF TABLES

Table		Page
I.	Results of Simulation in ϵ = 0.2	48
II.	Results of Simulation in ϵ = 0.4	49
III.	Results of Simulation in ϵ = 0.6	50
IV.	Results of Surge Flow Test	69
V.	Simulation Results of Surge Flow Test.	74
VI.	Simulation Results of Dynamic Flow Test.	75

LIST OF FIGURES

Figure		Page
1.	Filter Performance.	7
2.	Particle Transport Mechanism.	8
3.	Happel's Model.	13
4.	Schematic Diagram of the Limiting Trajectory. . . .	17
5.	Van Der Waal Forces	20
6.	The Fluid Pattern of Model.	28
7.	Limiting Trajectory	37
8.	Two Dimensional Plate	42
9.	U_0 Value	45
10.	The Effect of Porosity (N = 10)	51
11.	The Effect of Porosity (N = 20)	52
12.	The Effect of Porosity (N = 30)	53
13.	The Effect of Fiber Layer (ϵ = 0.2)	55
14.	The Effect of Fiber Layer (ϵ = 0.4)	56
15.	The Effect of Fiber Layer (ϵ = 0.6)	57
16.	The Effect of A	59
17.	Schematic of Multi-pass Filter Test Circuit	63
18.	Motorized Ball Valve.	64
19.	Typical Cyclic Flow Curve	65
20.	Surge Flow Test Results	70
21.	Test Results (Gehrking [37]).	71
22.	Experimental Results for Dynamic Flow	72

23. Different Magnitude Flow. 76

24. Comparison of Dynamic Test Data 1 with Simulation Results 77

25. Comparison of Dynamic Test Data 2 with Simulation Results 78

NOMENCLATURE

A the ratio of fluid viscous force to Van Der Waal force

a the radius of spherical particle

a_p particle size

a_s specific particle size

D capillary diameter

D_s the diameter of the unit cell

d distance between two spherical particles

E the modules of elasticity of the material

E_v Van Der Waal energy

F_v Van Der Waal force

f frequency of oscillation

f_g gravity force

g gravitational acceleration

h the thickness of the fiber plane

I_z the moment of inertia of the fiber plane

k constant

H Hamaker's constant

L fiber mat thickness

l the width of the pleat

M average flow rate

m mass of fluid

N the number of fiber layer

n_i number of inlet particle size greater than a_s

n_o number of outlet particle size greater than a_s

P magnitude of oscillation

p the hydrostatic pressure

p_∞ the uniform freestream pressure

Q fluid flow rate

q uniform load on the fiber mat plane

R collector radius

R_s unit cell radius

r the radius of spherical particle

s elongation of the plate

T torque

U fluid velocity

U_0 parameter for the elongation

V fluid superficial velocity

v the local mass average fluid velocity

z the vertical height of the point above plane

β filtration ratio

δ deflection

ϵ porosity of the filter

η_o initial filter efficiency

η total filter efficiency

μ fluid viscosity

ν Poisson's ratio

θ_e the angle of the particle enters the unit cell

ρ the local density of the fluid

ρ_f fluid density

ρ_p particle density

τ drag force

ω angle velocity

ψ flow stream function

∇ divergence

CHAPTER I

INTRODUCTION

A filter plays a very important role in the hydraulic system, because a good filter will keep the lubricants of the system clean and make the life of the system longer. Moreover, the cost of machine maintenance will decrease. In many areas the cost of machine maintenance is the first consideration to choose a hydraulic machine, so the designer can not omit any factor that can increase the cost. Therefore, the best design of a filter is not only to increase the efficiency and power of machinery, but also to try to decrease the cost of maintenance.

Essentially, an ideal filter can capture all the unwanted particles of the hydraulic fluid and keep the lubricants clean. Because the particles will continue to clog the filter, it is necessary to change or clean the filter periodically. In recent studies, some filters in good condition still can not get high efficiency [1]; that means, most particles can escape from the filtration process and can not be captured by the filter. If the harmful contaminants stay in the fluid, they are dangerous to the system and produce unanticipated results.

The particles in the lubricating oil which are not captured by the filter will circulate in the system. They are an important source of increasing wear and friction which will fail machine elements. Wear and friction are unavoidable whenever there is a relative motion between the particles and the internal surfaces of machines. Under these circumstances, it is necessary to provide an appropriate filter to remove damaging particles from the circulating fluid in the system. The efficiency of the filtration process is a standard way to judge a filter. Therefore, the solution of maintaining high efficiency is not to let critical particles escaped from the filter.

A filter is constructed of a pleated filter mat. Based on this structure, the porosity of the filter controls the size of the particles that can pass through the filter. The particles which escape capture are small and will not damage critical machine surfaces.

In considering the porosity, the important parameters that can influence the value of porosity must also be a concern. The number of fiber layers and the pore size distribution of the fiber mat are two critical parameters. Usually, filter designers in the development of a filter fit the system needs.

In actual practice, a filter can not necessarily provide performance needed in a system. This is especially true when the input flow is unsteady. Till now, most studies only discuss the effects of filter efficiency of

steady input flow, and the theoretical models are derived based upon constant flow. Some researches have reported filter performance data from experiments using cyclic flow, however, no analytical model has been presented for the unsteady flow conditions.

Throughout industry, most system designers usually depend on their individual expertise and experience to choose a filter for the system. This kind of assessment can not provide an effective and accurate way to control the system contamination level in a field environment. The reason why these selection technique are unsuccessful is due to insufficient knowledge concerning the filtration process under dynamic input flow.

This research presents the theoretical development of a cyclic flow filtration model. In order to accomplish the objective the model initially considers the filter under constant input flow. A parameter sensitivity is carried out by evaluating each critical parameter individually. In addition these parameters will be integrated into cyclic flow and compared with the filtration model. The final form of this model can predict the performance of a filter under different flow regimes. Experimental work is available to validate the model developed.

The remainder of this research presents and discusses the results of the entire research program. The next chapter discusses and outlines the previous investigations as they pertain to the concepts associated with filtration

process, fluid particle transport mechanisms, and filtration models. Chapter III presents the theoretical development of the filtration model under dynamic flow conditions. The experimental verification of the developed model and the results obtained from this research are illustrated in Chapter IV. Finally, Chapter V provides conclusions of this study, and recommendations for further studies.

CHAPTER II

PREVIOUS INVESTIGATIONS

Introduction

The filter performance of an operating machine has been recognized as a very important factor to affect system operation. Most system designers and machine operators realize that a filter is like a controlling element of the whole system. If this controlling element is poor, the system will get low efficiency. Therefore, there is a very rich amount of literature which discusses the filtration principal, filter application and filter model. However, very little research pays attention to investigate filter performance under dynamic flow condition.

This chapter reviews previous research reported relating to filtration process and filter model.

Filtration

Filtration has been one of the oldest separation methods since the ancient time in Egypt[2]. Records show that people used "fine" filtration to remove minute particles from water, wine and chemical solutions for several thousand years. The first filter for automobiles

was introduced in 1923. All the above descriptions prove that filter have been developed for a long time.

An ideal filter provides maximum resistance to stop the contaminants and offers minimum resistance to the system fluid flow. Furthermore, an ideal filter performance characteristic curve will be like Figure 1. In fact, there is no filter can completely separate particles from circulating fluid. Figure 1 shows the difference between an ideal filter performance and an actual one. Under this circumstance, there is a compromise between the degree of particle capture and escape. This is so called the efficiency of a filter. The efficiency of a filter represents the ability of a filter to remove particles from the system in the filtration process [3].

Filters use mechanical screens or porous media to capture particulate contaminants. The capture of entrained particles passing through a fibrous media is a very complicated phenomena involving the transport mechanisms of the particles as well as capture and retention mechanisms. Therefore, some of the principles of filtration mechanics are extremely important in the physics of filtration.

Understanding the motion of a particle when it moves through a fibrous medium is very useful to establish the conditions and assumptions of the model. A particle either passes through or is captured by the collector. Figure 2 illustrates several mechanisms which can occur in the filtration process. Fitch [2], Bensch [4], Rajagopalan [5]

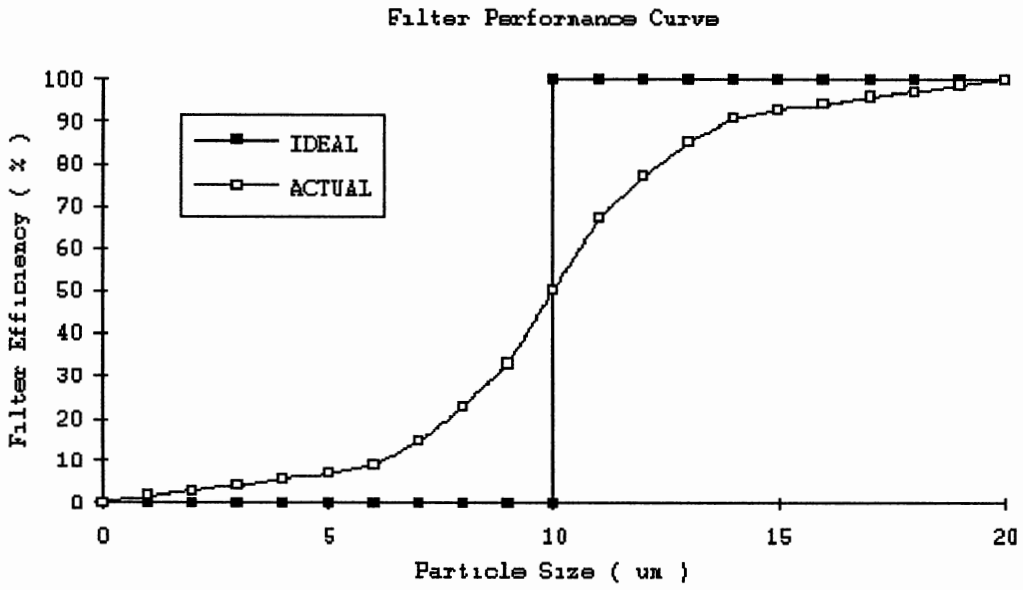

Figure 1. Filter Performance Curve

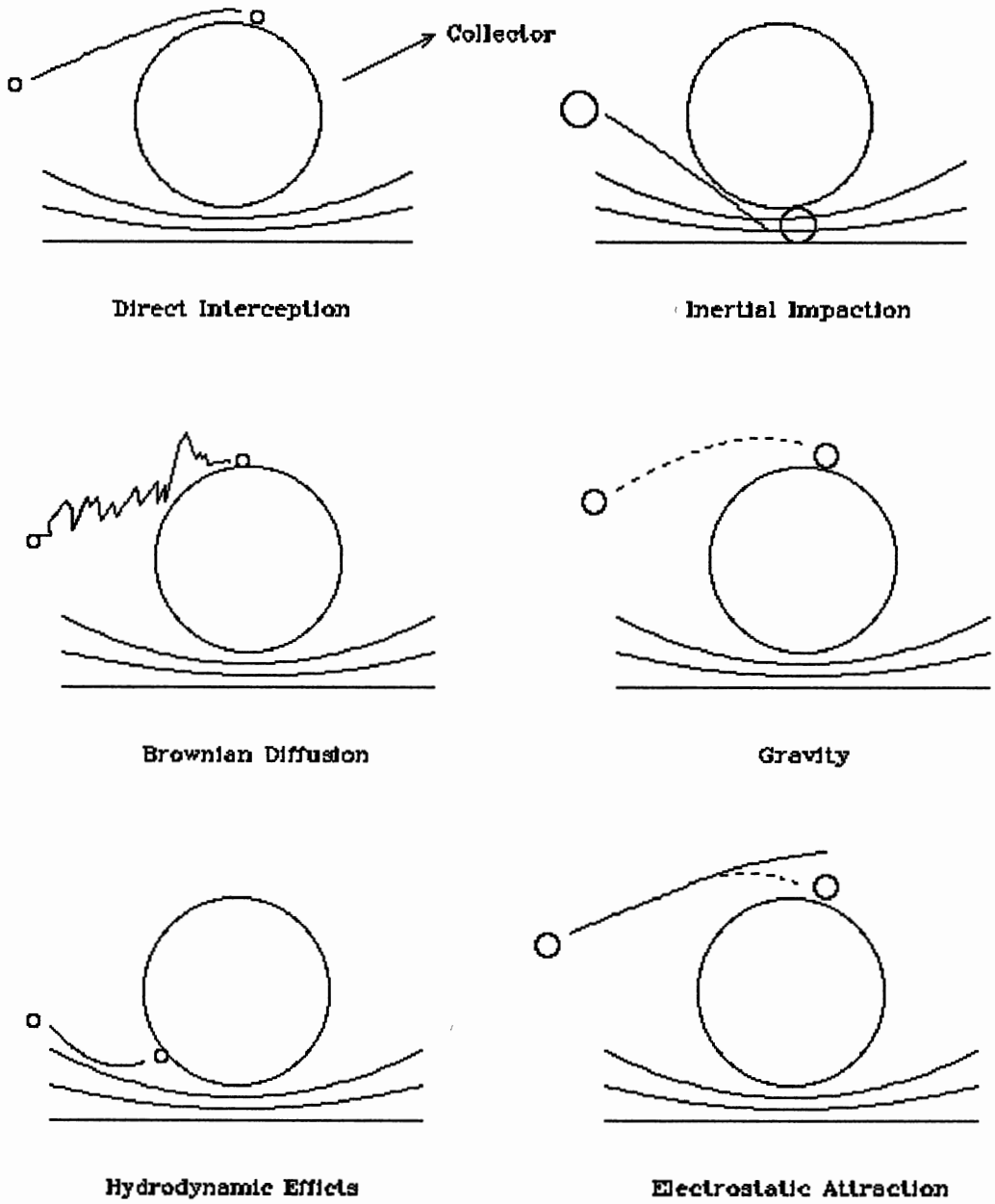

Figure 2. Particle Transport Mechanism

and Spielman [6] have discussed and categorized the particle mechanisms as follows:

Direct Interception

Inertial Impaction

Brownian Diffusion

Gravity

Hydrodynamic Effects

Electrostatic Attraction

The types of capture mechanisms involved will vary not only from one filter to another but also from one pore to another in a single fibrous medium. The effectiveness of each transport mechanism for various filtration modes must be estimated when a suitable model can be established.

Direct Interception

The particle follows a fluid streamline and does not deviate from that streamline. It is generally assumed that a particle will be captured if it comes within one particle radius of a collector. If this assumption is correct, it would be the only mechanism concerned in the filtration process. Then the filtration efficiency would be independent of the flow rate.

Inertial Impaction

If the density of the particle is much greater than that of the carrier fluid, the particle will not follow the same trajectory as the carrier fluid. Therefore, the

particle will deviate from the streamline when the fluid passes around the fibers. The effects of this mechanism are expected to increase with heavier particles and also to increase with flow rate through the medium.

Brownian Diffusion

When suspended particles are small enough, they will be significantly affected by the random molecular impingement of the surrounding fluid. Therefore, they do not move along a fluid streamline, but diffuse throughout the fiber mat. The effect of Brownian motion is increased with smaller particle sizes and decreased with higher fluid velocity. Brownian diffusion motion is always neglected when the diameter of particle is greater than one micron.

Gravity

If the density of the particle is different from that of the fluid, the particle will deviate from the fluid streamlines toward the ground direction because of gravity. Gravity effects will increase under low fluid velocity. It is normally neglected when the diameter of the particle is less than 25 to 30 microns [7].

Hydrodynamic Effect

According to the paper of Kitzmiller [8], there are many nonspherical particles in system fluids. Along with this situation nonuniformity of the flow field will cause

hydrodynamic effects. These effects will let the suspended particles migrate laterally in the filtration of highly nonspherical particles. It is known that most hydraulic systems have irregular shaped particles.

Electrostatic Attraction

If the particles possess a different charge from that of the filter fiber, they will be attracted by the filter fiber. This force is significant when the fluid velocity is low.

Particle retention is mainly due to the interference force between filter media and particles. When a filter model is developed, it is always very complicated and incorporated with a lot of ideal parameters. This restriction limits the study of filtration to be friendly, and no direct application can be easily obtained.

The filter efficiency is an important factor to be considered about the filtration process. For the efficiency of an ideal filter, the minimum particle size that will be captured depends on the design of the filter's pores and the operation of the system. Subsequently, the efficiency of a filter depends not only on fluid velocity and fluid temperature, but also to a significant degree on the density and size of the particle to be filtered [9]. Generally speaking, the smaller diameter fibers will have smaller pores and better efficiency [3]. But for the practical

filter, it is impossible to capture all the particles in the system fluid.

There are several ways to calculate the filter efficiency [10], one is called the Beta-ten ratio which was developed by Fitch [11]. The beta ratio at specific particle size a_s is defined as below

$$\beta(a_s) = \frac{n_i(a>a_s)}{n_o(a>a_s)} \tag{1}$$

where

a_s : specific particle size

n_i : number at the filter inlet particles greater than a_s

n_o : number at the filter outlet particles greater than a_s

Chapter IV will discuss the application of beta ratio in detail.

Filter model

It is very helpful to set up a filter model and simulate the results of a filtration process. A famous model was developed by Happel [12, 13, 14]. The basis of this mathematical model is that two concentric spheres can serve as the model for a random assemblage of spheres moving relative to a fluid. Figure 3 shows Happel's model. These spheres represent the particles of system fluid, and they are assumed to be of uniform size and smooth. The fluid

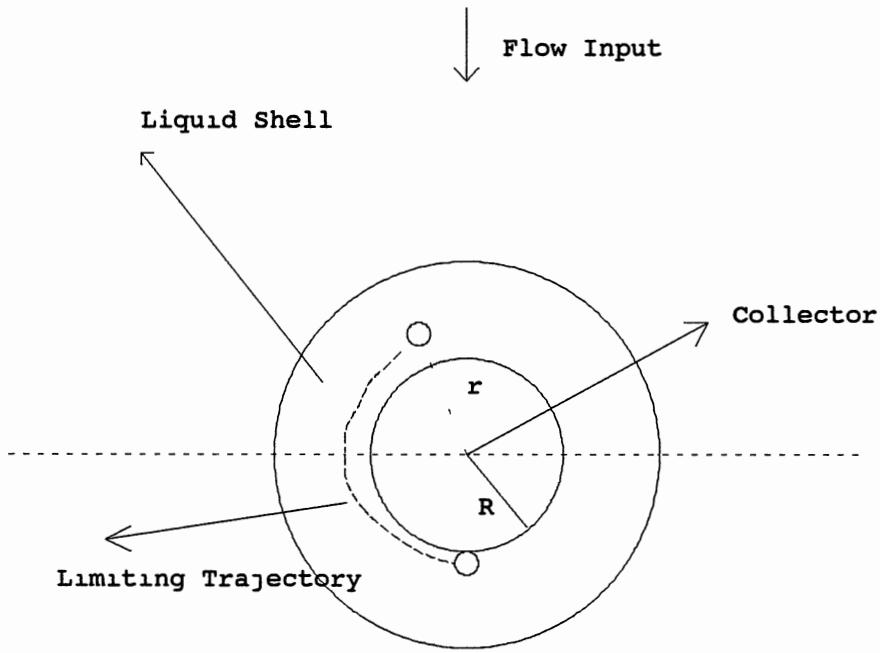

Figure 3. Happel's Model

motion in Happel's model is at low Reynold's numbers, and the Navier-Stokes equations with the inertia terms neglected are used to describe the process [15]. The solution of this model predicts the pressure drop across the fiber mat as a function of fractional void volume.

The principle of Happel's model is widely used in other's model. Yao's work followed Happel's principle and formulated a trajectory equation for the particle transport toward the fibers by considering some of the most important transport mechanism mentioned in the last section [16, 17]. From Yao's work, one of the most important simplifications used in subsequent theoretical investigations is the omission of the contribution of the deposition rate due to inertia effect of the particle, because the inertia effect of the particle in water filtration is insignificant. Yao also develops the single collector concept which can be very successful in estimating the particle retention of the filter.

There is a major defect in the single collector model. That is, it can not describe the pressure drop across the fiber mat as a function of the porosity. Therefore, some models have been developed recently to change the single collector to the so-called "pressure drop model" [18, 19, 20, 21]. Most experimental works have shown that the pressure drop across a filter with low Reynold number fluid flow follows the D'arcy's equation which as shown below

$$\Delta p = k \mu VL \tag{2}$$

where

Δp : pressure drop

k : constant

μ : fluid viscosity

V : fluid superficial velocity

L : fiber mat thickness

The efforts of many authors tried to relate the constant of proportionality, k, to the physical properties of the filter medium [22]. One approach is to consider that the fibrous media consists of many small capillary tubes, and the pressure drop can be determined from a variation of the Hagan-Poiseuille law which can be written as follows:

$$\Delta p = \frac{128 \mu LQ}{\pi D^4} \tag{3}$$

where

Q : fluid flow rate

D : capillary diameter

Application of this equation is complicated because several critical parameters are not included in this equation. For example, the flow paths are not straight and the cross-sectional areas of the capillaries are not uniform throughout the medium. Furthermore, the pores tend to be non-circular [23].

FitzPatrick uses the Happel's cellular model and his research contains an extensive experimental analysis [24]. In his experimental work, not only a wide range of particles and fiber sizes are covered, but also the conditions of his experiment are controlled accurately. Payatakes, Tien and Rajagopalan coordinate the Happel's model with the experimental data from FitzPatrick to develop a limiting trajectory model [25]. In this model they try to characterize the filter by its hydrodynamic behavior and by its role as the collector to capture the particles. Furthermore, they use this model to predict the dynamic behavior of the filtration process, that is, to predict the results when the input flow and the pressure drop across the filter are changed. Figure 4 is the model of Rajagopalan and Tien.

Tichy's model is very similar to Rajagopalan and Tien's model [26]. This steady state model is proposed for the filter of a simple lubrication system consisting of an engine and a filter [27]. Tichy suggests that for an optimum filter all particles are captured above a particular "cut-off" size and none below that size. Whenever the particle size increases, the capture of fractional particles increases also. The cut-off size can be determined by a series of field tests.

The trajectory concept is used in both Rajagopalan and Tichy's models. It reveals that when a fluid passes through a filter, the surface of the filter medium may capture the

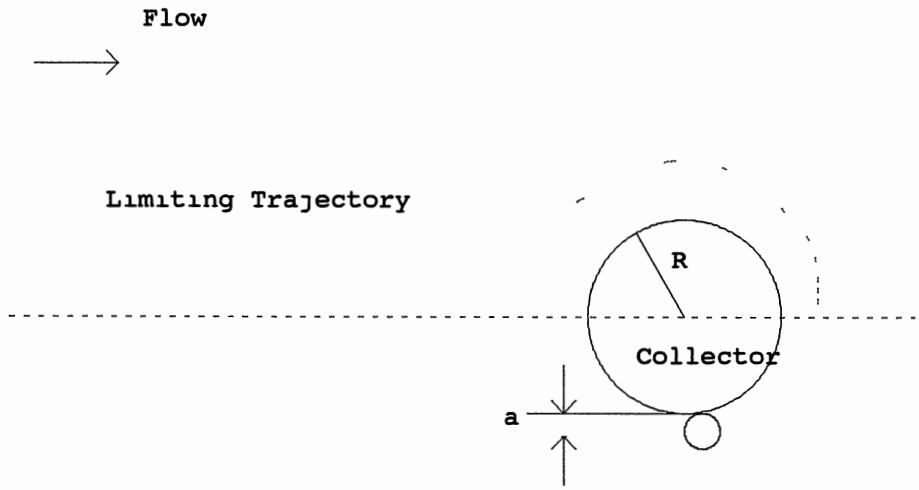

Figure 4. Schematic Diagram of Limiting Trajectory

particles. Such capture is caused by various mechanisms, the four most important mechanisms are diffusion, interception, gravitational collection and collection due to surface forces. All of the above mechanisms except the surface force have been explained in the last section. The particle trajectory equation is obtained by using a force balance on this particle. If the trajectory of a particle intercepts the collector, then the particle is assumed to be captured.

There is a little difference between any of these models. The primary differences lies in the forces selected and considered. Omitting the insignificant forces, there are three very critical kinds of forces given as follows:

Gravity Force

London Force

Viscous Force

Because different forces selected and neglected will influence the accuracy of the model, the model can be applied only under some conditions. It is important to consider the significant ones in developing the model.

Gravity Force

The characteristic of the gravity has been described previously, and from Rajagopalan [5] and Spielman [7] the force f_g can be formulated as

$$fg = \left[\frac{4}{3} \right] \pi ap^3 (\rho_p - \rho_f) g \qquad (4)$$

where

a_p : particle size

ρ_p : particle density

ρ_f : fluid density

g : gravitational acceleration

The gravity force shown in Equation (4) is usually small enough to be neglected in practical models.

London Force

Of the many inter-molecular forces, only the Van Der Waals forces are considered in previously reported models. These forces involve various phenomena such as surface tension, physical adsorption and even adhesion between solid surface in contact [28]. These phenomena are caused by the instantaneous dipole moments generated by the temporary asymmetry in the distribution of electrons around the nucleus. The characteristic parameter of this interaction is called the Hamaker's constant [29], H, and it is of the order of 10^{-12} to 10^{-13} ergs. Hamaker discussed Van Der Waals adhesive forces in both liquids and in aerosols. He derived the equations by finding the forces between two spherical particles, or a spherical particle and a large flat plate as shown in Figure 5. These equations use the energy E_v and force F_v, and they can write as

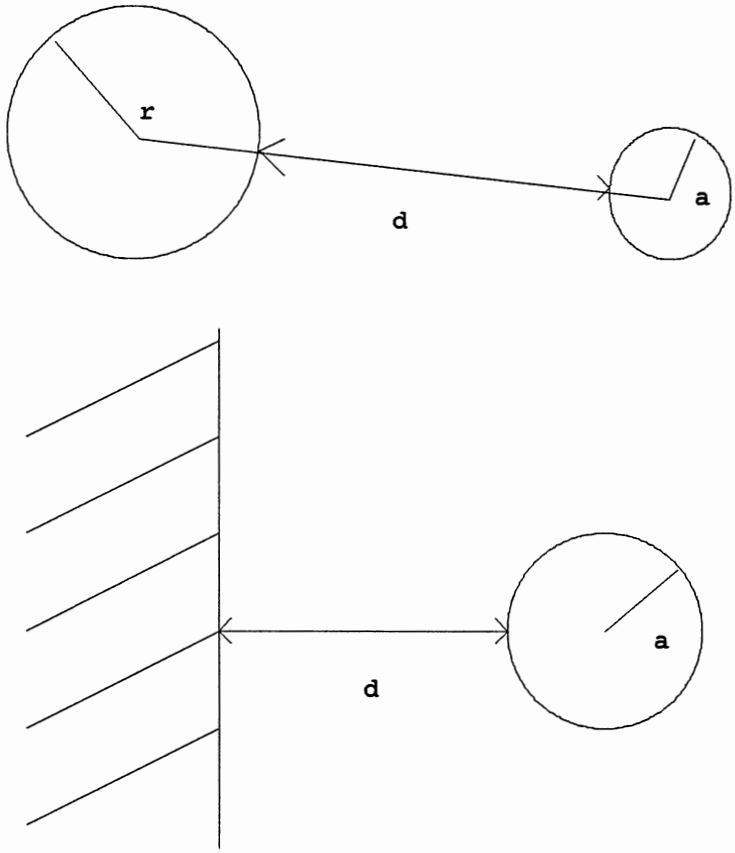

Figure 5. Van Der Waals Forces

$$E_V = -\frac{H}{12}\left[\frac{y}{x^2 + xy + x} + \frac{y}{x^2 + xy + x + y}\right] - \frac{H}{12}\left[2\ln\frac{x^2 + xy + x}{x^2 + xy + x + y}\right] \tag{5}$$

where

H : Hamaker's constant

a, r : the radius of spherical particle

d : distance between two spherical particles

$x = \frac{d}{2r}$

$y = \frac{a}{r}$

The application of this Equation (5) depends on the value of x and y. If y is equivalent to two spherical particles, Equation (5) can be simplified and converted to the force mode instead of energy. It can be written as

$$F_V = -\frac{H}{6}\left[\frac{2(x + 1)}{x^2 + 2x} - \frac{x + 1}{(x^2 + 2x)^2} - \frac{2}{x + 1} - \frac{1}{(x + 1)^3}\right] \tag{6}$$

Equation (6) can be approximated by using H, and the radius of the particle to represent the force between a small spherical particle and a large one [3]. Therefore, the typical equation of Van Der Waals forces is

$$F_V = -\frac{2}{3}\frac{Ha^3}{((d - r) + a)^2((d - r) - a)^2} \tag{7}$$

These forces act only in the radial direction of the particle, and they are always neglected in the flow field except for a region very close to the collector. Just as Tichy [27] said, for nonpolar molecule fluids, such as petroleum oils, it is doubtful that these forces play a significant role.

Viscous Force

The viscous forces effects are extremely complex. Since the undisturbed fluid velocity will increase with the distance away from the collector, the fluid flow has a lower local velocity at the leading edge of the particle than on the trailing edge. Therefore, this velocity difference produces a torque on the particle, causing the particle to rotate in the r - θ plane. In order to simplify this complicated situation, the conception of creeping flow are used. The Navier-Stokes equations can be applied to describe the viscous forces effects [15].

$$\rho \frac{Dv}{Dt} = - \nabla(p + \rho g z) + \mu \nabla^2 v \qquad (8)$$

where

ρ : the local density of the fluid

∇ : the divergence

μ : shear viscosity

p : the hydrostatic pressure

v : the local mass average fluid velocity

z : the vertical height of the point above plane

If the model assumes that only the viscous force and London forces will be considered, then Equation (8) can be rewritten as

$$\rho\frac{Dv}{Dt} = \rho\left(\frac{\partial v}{\partial t} + v\nabla v\right) = -\nabla p + \mu\nabla^2 v + \rho F \tag{9}$$

where

F : external body force on element

Assuming that the Reynolds number is less than one, it is necessary to consider the creeping motion in the fluid. The creeping motion equations may generally be used when $\rho\, v\cdot\nabla v$ is small as compared to $\mu\nabla^2 v$ at each point of the fluid. Since the inertia term is omitted, the creeping motion of a speed U which passes a sphere of radius a is convenient to find the solution. Under this situation, the stream function will be written as

$$\psi = \frac{1}{4}\, Ua^2\sin^2\theta\left(\frac{a}{r} - \frac{3r}{a} + \frac{2r^2}{a^2}\right) \tag{10}$$

The velocity components which use the spherical polar coordinates are

$$u_r = U\cos\theta\left(1 + \frac{a^3}{2r^3} - \frac{3a}{2r}\right) \tag{11}$$

$$u_\theta = U\sin\theta\left(-1 + \frac{a^3}{4r^3} + \frac{3a}{4r}\right) \tag{12}$$

When u_r and u_θ are known, the pressure can be expressed by

$$p = p_\infty - \frac{3\mu aU}{2r^2}\cos\theta \tag{13}$$

where

p_∞ : the uniform freestream pressure

At this time, the pressure is proportional to μ, antisymmetric, positive at the front and negative at the rear of the sphere. Therefore, the pressure will create a pressure drag on the sphere. Besides the pressure drag force, there is a surface shear stress which creates a drag force also, and it can be represented as

$$\tau_{r\theta} = -\frac{U\mu\sin\theta}{r}\left[1 - \frac{3a}{4r} + \frac{5a^3}{4r^3}\right] \tag{14}$$

Therefore, the total drag forces can be found by integrating the pressure drag force and surface shear stress as follows:

$$F = 4\pi\mu Ua + 2\pi\mu Ua = 6\pi\mu Ua \tag{15}$$

This is the Stokes' law formula which it describes the drag force on a sphere of radius a in an unbound fluid which has a velocity U. Similarly, if the fluid is rotating at speed ω, it is easy to find the torque T from the following expression:

$$T = 8\pi\mu a^3\omega \tag{16}$$

where T acts in the same direction as in the sphere rotation vector. The same form of Stokes' law is applied whenever the sphere is moving and the fluid is stationary.

If the radius of the sphere is small like a particle and the inertia force between two spheres in the fluid is neglected, the viscous effect is linear. The system can be separated into a stationary particle in a moving fluid or a moving particle in a stationary fluid. Under this situation, the solution of the viscous force in system can found by superimposing these two conditions.

Goldman [30, 31], Bernner [32], O'Nell [33] and Goren [34, 35] have all discussed the effect of viscous forces on a particle moving in the neighborhood of an obstacle, and a detailed discussion will be in the next chapter.

As in the above description, most of previous models only considered the filtration process under steady flow. For the filtration process of dynamic flow condition, there are only experimental data to reveal the effects. However, most hydraulic filters, especially when installed in the return lines of hydraulic system, seldom operate under steady flow condition.

There have been many tests proposed to evaluate the separation characteristics of a filter under dynamic flow [36, 37, 38, 39, 40, 41]. Their studies found the filter performance will be dramatically reduced after some critical parameters are changed. These parameters include temperature, viscosity, and flow rate [42]. The change in

flow rate has been shown to have a very significant effect upon filter performance. In an actual hydraulic system, the flow rate is not constant but varies significant. This varying flow rate is called surge flow. The surge flow into the reservoir as a cylinder retracts or a pressure control valve unloads can increase flow through the filter which is several times higher than the system design flow rate. In addition an on-off machine cycle can provide surge flows.

In order to understand the problems of surge flow, it is necessary to develop a theoretical model to simulate the actual hydraulic system filter. The previous work has established the basis to develop a suitable model and explain filter performance under dynamic flow. Details of the theoretical development are illustrated in the next chapter.

CHAPTER III

DEVELOPMENT OF DYNAMIC FILTRATION MODEL

Introduction

This chapter outlines the conceptual development of the filtration theory. There are two important steps to start a theoretical analysis of a filter model:

1. To select an appropriate porous media model to characterize the filter for its fluid mechanical behavior.
2. To choose a suitable theoretical technique to estimate the rate of particle retention.

The basic approximate principle of the filter model has described in the last chapter. This chapter presents the theoretical model under steady flow and dynamic flow conditions.

Model Flow Pattern

The fluid pattern of the model is shown in Figure 6. The fiber mat consists of the collectors like spheres which are uniformly distributed, and the diameters of the fibers that are represented by the collectors are also uniformly distributed. The unit cell, like an insulator, surrounds a collector and does not interfere with cells. When the

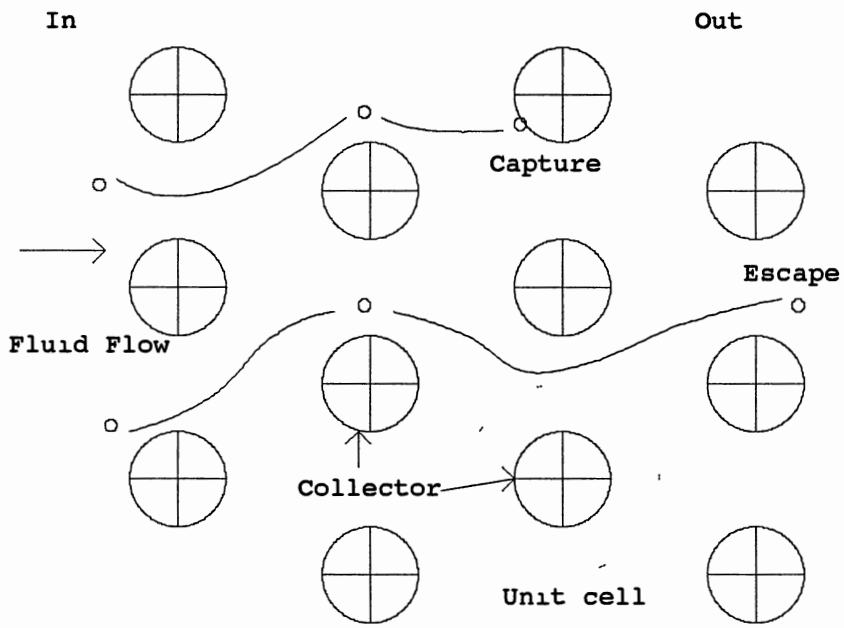

Figure 6. The Fluid Pattern of Model

suspended particles enter the collector, they will either collide with the collector or escape from the collector. The model assumes that particles will be attached on the collector, if the particles touch the collector. At this time, London forces are large enough to overcome fluid viscous forces. It is obvious that the most critical particle capture mechanisms considered in the model are the direct interception and surface forces.

The model assumes that the total filter efficiency is the same as the unit cell efficiency. In addition the porosity of the unit cell is the same as the porosity of the total filter. The relation between the collector radius and the unit cell radius can be shown that:

$$R_S = R \left(\frac{1}{(1 - \epsilon)^{1/3}} \right) \tag{17}$$

where

R_S : unit cell radius

R : collector radius

ϵ : porosity

The velocity external of the spherical collector is obtained under the condition that the fluid is stationary and the solid moves through it with some velocity. The equation of the motion for the creeping flow is found by using Stoke's law which is for Reynolds number less than one and following the boundary conditions as below

1. The radial velocity at outer surface of the unit cell is zero.
2. The tangential stress at the outer surface is zero.
3. There is no slip condition at the particles and fluid boundary.

Under these boundary conditions, the formula of the flow stream function for the region $R \leq R_p \leq R_s$ is given by [25, 43]

$$\psi = \left(\frac{V}{2} \right) \sin^2\theta R^2 \left(\frac{K_1}{\underline{R}_p} + K_2\underline{R}_p + K_3\underline{R}_p^2 + K_4\underline{R}_p^4 \right) \tag{18}$$

where

$$\underline{R}_p = \frac{R_p}{R}$$

$$K_1 = \frac{1}{W}$$

$$K_2 = \left(\frac{3 + 2p^5}{W} \right)$$

$$K_3 = p \left(\frac{3 + 2p^5}{W} \right)$$

$$K_4 = - \frac{p^5}{W}$$

$$W = 2 - 3p + 3p^5 - 2p^6$$

$$p = (1 - \epsilon)^{1/3}$$

Spherical coordinates are used in the model. The location of the particle is given by (R_p, θ_p) where R_p is the

distance from the particle center to the collector center. If these coordinates are changed to the dimensionless coordinates, the parameters will be given as follow:

$$z = R_p - R$$

$$\underline{z} = \frac{(R_p - R)}{a}$$

where

a : the radius of particle

Under these dimensionless parameters, the fluid velocity from Equation (19) can be approximated to r & θ directions.

$$\underline{v}_r = - B\underline{a}^3\underline{z}^2\cos\theta_p \tag{19}$$

$$\underline{v}_\theta = B\underline{a}^2\underline{z}\sin\theta_p + C\underline{a}^3\underline{z}^2\sin\theta_p \tag{20}$$

where

$$\underline{a} = \frac{a}{R}$$

$$B = \frac{3 - 3p^5}{W}$$

$$C = \frac{-\frac{7}{2} - 3p^5}{W}$$

Equations (11) and (12) are valid when the particle is very close to the collector. This fluid velocity is derived based on the axisymmetric stagnation flow that is normal to

the collector, the linear shear flow, and the parabolic shear flow.

Force and Moment of the Model

There are several important forces that occur in the process, and the characteristics of these forces have been described in Chapter II. The force and moment balance equations of a particle moving around the collector in the spherical coordinates can be shown as follows:

$$F_r^n + F_r^t + F_r^r + f_r^s + f_r^l + f_r^p + F_v = 0 \tag{21}$$

$$F_\theta^n + F_\theta^t + F_\theta^r + f_\theta^s + f_\theta^l + f_\theta^p = 0 \tag{22}$$

$$T_\varphi^n + T_\varphi^t + T_\varphi^r + t_\varphi^s + t_\varphi^l + t_\varphi^p = 0 \tag{23}$$

where the capital alphabet F and T represent the forces on a moving particle in a stationary fluid, and the small alphabet f and t represent the forces on a stationary particle in a moving fluid. The definitions of the superscripts are as follow:

t : particle translates tangential to sphere

n : particle translates normal to sphere

r : particle rotates with axis parallel to sphere

l : linear shearing fluid flow

p : parabolic shearing fluid flow

s : axisymmetric stagnation fluid flow toward the collector

$$F_r^n = - \underline{F}_r^n 6\pi\mu a(u_r) \tag{24}$$

$$F_\theta^t = - \underline{F}_\theta^t 6\pi\mu a(u_\theta) \tag{25}$$

$$F_\theta^r = \underline{F}_\theta^r 6\pi\mu a^2\omega \tag{26}$$

$$f_r^s = - \underline{f}_r^s 6\pi\mu a[VB(y^2)\cos\theta_p] \tag{27}$$

$$f_\theta^l = \underline{f}_\theta^l 6\pi\mu a[VB(y)\sin\theta_p] \tag{28}$$

$$f_\theta^p = \underline{f}_\theta^p 6\pi\mu a[VC(y^2)\sin\theta_p] \tag{29}$$

$$T_\varphi^t = \underline{T}_\varphi^t 8\pi\mu a^2(u_\theta) \tag{30}$$

$$T_\varphi^r = - \underline{T}_\varphi^r 8\pi\mu a^3\omega \tag{31}$$

$$t_\varphi^l = \underline{t}_\varphi^l 8\pi\mu a^2 \left[V\frac{B}{2}\sin\theta_p \right] \tag{32}$$

$$t_\varphi^p = \underline{t}_\varphi^p 8\pi\mu a^2[VC(y)\sin\theta_p] \tag{33}$$

$$F_\theta^n = F_r^t = F_r^r = f_\theta^s = f_r^l = f_r^p = T_\varphi^n = t_\varphi^s = 0 \tag{34}$$

where

$y = \underline{a}z_p$

$\underline{F}_r^n$, $\underline{F}_\theta^t$, $\underline{F}_\theta^r$, $\underline{f}_r^s$, $\underline{f}_\theta^l$, $\underline{f}_\theta^p$, $\underline{T}_\varphi^t$, $\underline{T}_\varphi^r$, $\underline{t}_\varphi^l$, $\underline{t}_\varphi^p$: correction factors from the experiment [5].

The Particle Trajectory Equation and Efficiency

The formulation of the trajectory equation is based on the assumption that the particle concentration is sufficiently low. Therefore, the motion of any given

particle does not interfere with that of the others. The trajectory equation can be found by solving the forces and torques equilibrium Equations (21) to (23). It is convenient to substitute Equations (24) to (34) and Equation (7) to these connected equations and rearrange those equations to the nondimensional forms as below

$$\underline{T}_{\varphi}{}^{t}(\underline{u}_{\theta}) - \underline{T}_{\varphi}{}^{r}(a\omega) + \underline{t}_{\varphi}{}^{l}\left[\frac{B}{2}\sin\theta_p\right] + \underline{t}_{\varphi}{}^{p}(Cy\sin\theta_p) = 0 \tag{35}$$

$$-\frac{1}{A}\frac{1}{(\underline{z}_p - 1)^2(\underline{z}_p + 1)^2} - \underline{F}_r{}^{n}(\underline{u}_r) - \underline{f}_r{}^{s}(By\cos\theta_p) = 0 \tag{36}$$

$$-\underline{F}_{\theta}{}^{t}(\underline{u}_{\theta}) + \underline{f}_{\theta}{}^{l}(By\sin\theta_p) + \underline{f}_{\theta}{}^{p}(Cy^2\sin\theta_p) + \underline{F}_{\theta}{}^{r}(a\omega) = 0 \tag{37}$$

where

$$\underline{u}_{\theta} = \frac{u_{\theta}}{V}$$

$$\underline{u}_r = \frac{u_r}{V}$$

$$A = \frac{9\pi\mu R^2 V}{H}$$

Rearrange Equations (35) to (37) to solve $\underline{u}_{\theta}$ and $\underline{u}_r$, and from Equation (36) can get:

$$\underline{u}_r = \frac{1}{\underline{F}_r{}^{n}}\left[-\frac{1}{A}\frac{1}{(\underline{z}_p - 1)^2(\underline{z}_p + 1)^2} - \underline{f}_r{}^{s}(By^2\cos\theta_p)\right] \tag{38}$$

from Equation (35)$\cdot\underline{F}_{\theta}{}^{r}\ \frac{1}{\underline{T}_{\varphi}{}^{r}}$ + Equation (37) can find:

$$\underline{u}_\theta = \frac{1}{g_3} \sin\theta_p \left[g_1 \frac{C}{2} + g_2(Dy) + \underline{f}_\theta{}^l(Cy) + \underline{f}_\theta{}^p(Dy^2) \right] \quad (39)$$

where

$$g_1 = \frac{\underline{t}_\varphi{}^l \underline{F}_\theta{}^r}{\underline{T}_\varphi{}^r}$$

$$g_2 = \frac{\underline{t}_\varphi{}^p \underline{F}_\theta{}^r}{\underline{T}_\varphi{}^r}$$

$$g_3 = \frac{\underline{F}_\theta{}^t \underline{T}_\varphi{}^r - \underline{T}_\varphi{}^t \underline{F}_\theta{}^r}{\underline{T}_\varphi{}^r}$$

If the coordinates of the particle will be considered to replace the fixed spherical coordinates, the trajectory equation can use $\underline{z}_p$ and θ_p. The relationships between the particle and the velocity are

$$\underline{u}_r = \frac{d\underline{r}_p}{dt} \quad (40)$$

$$\underline{u}_\theta = \underline{r}_p \frac{d\theta_p}{dt} \quad (41)$$

where

$$\underline{r}_p = y + 1 = \underline{a}\underline{z}_p + 1$$

Dividing Equation (40) by Equation (41) and finding

$$\frac{d\theta_p}{d\underline{r}_p} = \frac{1}{\underline{r}_p}\frac{\underline{u}_\theta}{\underline{u}_r}$$

$$= \frac{\underline{F}_r{}^n \sin\theta_p}{g_3\underline{r}_p} \quad .$$

$$\left[\frac{g_1(\frac{B}{2}) + g_2[C(\underline{r}_p - 1)] + \underline{f}_\theta{}^l[B(\underline{r}_p - 1)] + \underline{f}_\theta{}^p[C(\underline{r}_p - 1)^2]}{-\frac{1}{A}\frac{1}{(\frac{\underline{r}_p - 1}{\underline{a}} - 1)^2(\frac{\underline{r}_p - 1}{\underline{a}} + 1)^2} - \underline{f}_r{}^s[B\cos\theta_p(\underline{r}_p - 1)^2]}\right] \tag{42}$$

The solution of Equation (35) as a function of several parameters can be expressed as

$$\theta_p = \theta_p(\underline{r}_p, \underline{a}, A, B, C, \underline{r}_{p0}, \theta_{p0}) \tag{43}$$

where $\underline{r}_p$ and θ_p are the initial conditions in which the particle will be captured by the unit cell. The B and C are functions of porosity ϵ, so they can be replaced by ϵ. Finally, Equation (43) can be rewritten as

$$\theta_p = \theta_p(\underline{r}_p, \underline{a}, A, \epsilon, \underline{r}_{p0}, \theta_{p0}) \tag{44}$$

Equation (44) can represent the trajectory of a given particle. To determine the collection efficiency of the model, it is unnecessary to calculate the trajectory of all the particles that pass the model. The concept of limiting trajectory will apply to the model shown in Figure 7, and the procedure of this method only calculates the trajectory of the specific size particle which is just captured by the collector. The last point of the collector which captures

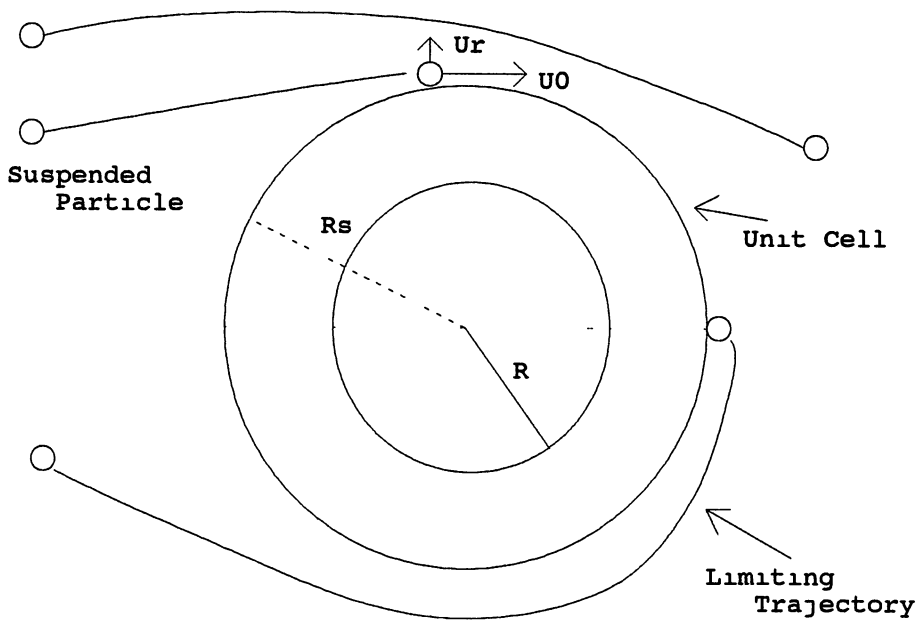

Figure 7. Limiting Trajectory

the particle is at $\theta_{p0} = \pi$ and $\underline{r}_{p0} = 1$, and the first point of the particle which just enters the unit cell is at $\theta_p = \theta_e$ and $\underline{r}_p = \frac{R_s}{R} = (1 - \epsilon)^{-1/3}$. Substituting them to Equation (44) results in the following:

$$\theta_e = \theta_p[(1 - \epsilon)^{-1/3}, 1, \pi, \underline{a}, \epsilon, A] \tag{45}$$

The θ_p of the specific size particle which enters to the unit cell needs to compare with θ_e. The particle will be captured by the collector, if the θ_p of the particle is smaller than θ_e; however, the particle will escape from the unit cell, if the θ of the particle is larger than θ_e. Therefore, the fluid flow passes through the unit cell and belongs to the circular cross section enclosed by the limiting trajectory, and the particle inside the cross section will be captured. The formula is

$$(\text{volume / unit time}) = \pi(R_s \sin\theta_e)^2 U \tag{46}$$

Since $\pi R_s^2 U$ represents the total volumetric flow rate through the unit cell, the initial efficiency η_0 of the unit cell is

$$\eta_0 = \frac{(\pi R_s^2 \sin^2\theta_e U)}{(\pi R_s^2 U)} = \sin^2\theta_e \tag{47}$$

Equation (47) can also be written as the function of these parameters:

$$\eta_0 = \eta_0(\underline{a}, \epsilon, A) \tag{48}$$

Considering the multiple layers of the fibers, the total efficiency will be changed by the number of the fiber layers. If the length of a filter is L, the number of the fiber layers in the filter is

$$N = \frac{L}{D_s} \tag{49}$$

where

N : the number of fiber layer

D_s : the diameter of the unit cell

Therefore, the total efficiency can be rearranged by substituting Equation (49) to Equation (48).

$$\eta = 1 - (1 - \eta_0)^N \tag{50}$$

where the escapable particle efficiency of each single layer is $(1 - \eta_0)$, after N layers, the total escapable particle efficiency will be multiplied itself N times, and then it becomes $(1 - \eta_0)^N$. Finally, the collection efficiency is equal to one minus $(1 - \eta_0)^N$. Equation (50) will apply under the following conditions.

1. If the suspended particle moves very closely or, even touches the collector, it will be captured by the collector and unable to escape from the collector. At this time, the Van Der Waals forces

will overcome all the other forces and become infinite [44].

2. A model of an idealized mat, where the fiber are everywhere perpendicular to the direction of flow, is assumed by the fibers that act individually and do not interfere with others. Under these conditions, the collection efficiency of the model will be a approximate summation of the collection efficiencies of the individual fiber.
3. The structure of every fiber layer is the same and includes the porosity of the fibers, the density of the fiber and so on. Therefore, the total collection efficiency can be found by superimposing the collection efficiency of each single layer.

Dynamic Flow Model

Equation (48) shows that the collection efficiency only considers the particles size of contaminants, the porosity of the filter, and the value of A. In the steady flow input, the porosity of the filter is assumed a constant. If a unique particle size is selected and the viscosity is fixed, the porosity will become larger under the dynamic flow rate. This has been proven by the experimental data reportedly Bensch [42]. When the porosity of the filter increases, the collection efficiency of this filter decreases. The reason is that the larger porosity which has the larger space between two fibers will let the larger

particles pass through the filter. Therefore, it is helpful to develop a formula to represent the change of the porosity under the dynamic flow condition.

It is reasonable assumption that the larger porosity during surge flow will influence the forces and moments acting on the filter and cause the fiber mat of the filter elongate. The force on the fiber mat is given by

$$F_{total} = F_{steady} + \Delta F \tag{51}$$

The force change ΔF is produced by the momentum change caused by flow surges and can be expressed as

$$\Delta F = \frac{m \Delta V}{\Delta t} \tag{52}$$

where

m : mass of fluid

ΔV : the change of fluid velocity

If the pleat of the filter is assumed to be as a two-dimension plate as shown Figure 8, the deflection of this plate can be formulated in x_o - y_o Cartesian coordinates by the following:

$$y_o = \frac{4\delta x_o(l - x_o)}{l^2} \tag{53}$$

where

δ : the maximum deflection

l : the width of the pleat

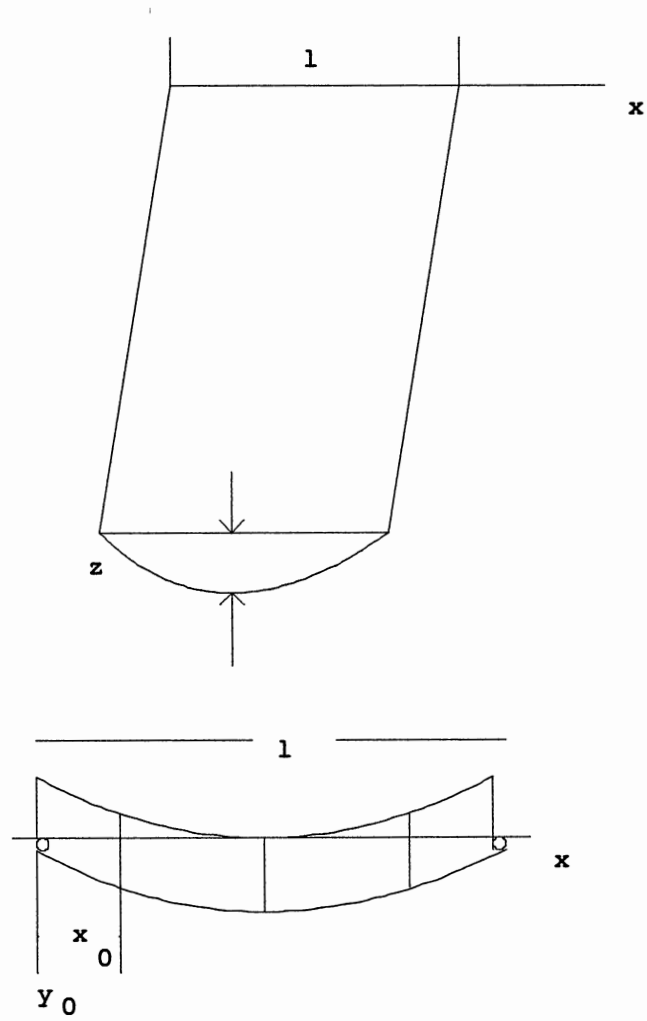

Figure 8. Two Dimensional Plate

The maximum deflection of the filter pleat is located on the center line of the pleat and occurs when the flow rate is varying from zero to the highest rate. The largest flow rate difference causes the maximum momentum change. Therefore, the new width of the filter pleat can be obtained by the equation as below

$$s = 2\int_0^{\frac{1}{2}} \sqrt{dx_o^2 + dy_o^2} \tag{54}$$

$$= 2\int_0^{\frac{1}{2}} \left[\sqrt{1 + \left(\frac{dy_o}{dx_o}\right)^2} \right] dx_o \tag{55}$$

Because $\frac{dy_o}{dx_o}$ is very small, Equation (55) can change to

$$s = 2\int_0^{\frac{1}{2}} \left[1 + \frac{1}{2}\left(\frac{dy_o}{dx_o}\right)^2 \right] dx_o \tag{56}$$

Then, Equation (53) can make derivation with y and then substitute to Equation (56). Finally, the length of the deflection curve caused by the maximum pressure acting on the fiber plane is

$$s = l\left(1 + \frac{8}{3}\frac{\delta^2}{l^2}\right) \tag{57}$$

In Equation (57), the elongation of the fiber plane in the wide direction is $\frac{8}{3}\frac{\delta^2}{l^2}$, and the maximum deflection δ obtained from Timoshenko [45, 46] is

$$\delta = \frac{5ql^4}{384EI_z} f(u) \tag{58}$$

where

q : uniform load on the fiber mat plane

E : the modules of elasticity of the material

I_z : the moment of inertia of the fiber plane

In Equation (58), the f(u) will be introduced to calculate the maximum deflection δ, and it is formulated as

$$f(u) = \frac{\operatorname{sech}(u) - 1 + \frac{u^2}{2}}{\frac{5u^4}{24}} \tag{59}$$

where u can be obtained from Figure 9 in [45], and in Figure 9, U_0 can be written as

$$U_0 = \left(\frac{E}{(1 - \nu^2)q}\right)^2 \left(\frac{h}{l}\right)^8 \tag{60}$$

where

ν : Poisson's ratio

h : the thickness of the fiber plane

Equations (53) to (60) show the formulas which describe the elongation of fiber mat plane. The assumption of the fiber

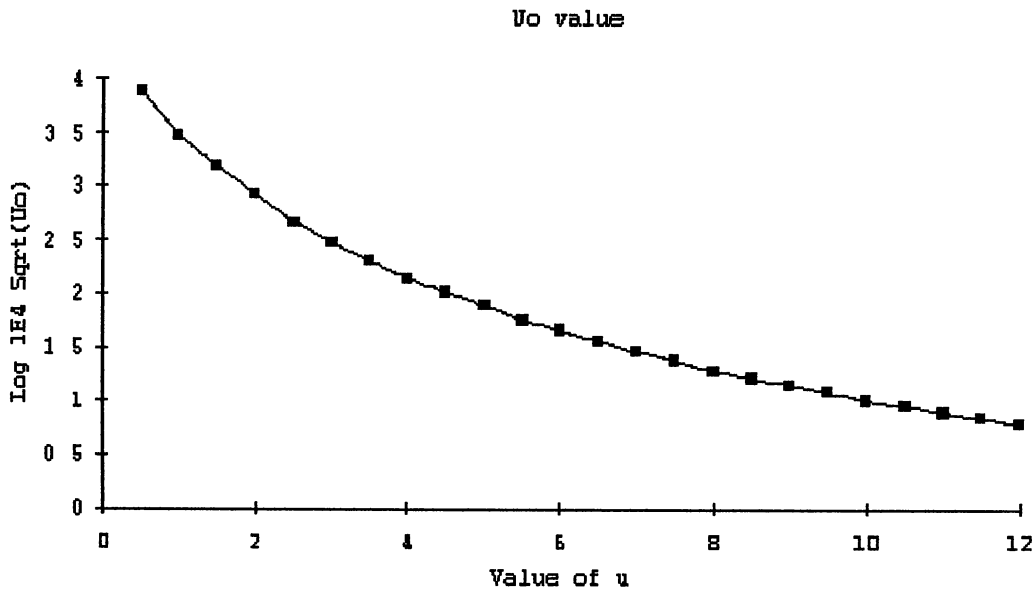

Figure 9. U_0 value

mat plane under the dynamic flow input is that only the space between two fibers gets larger, and the diameter of the fiber remains unchange. Because the space gets larger, the porosity of the fiber mat increases. In the above explanation, the collection efficiency of the filter will decrease. The new porosity under the dynamic flow input can be obtained by recalling Equation (17) and rearranging to

$$\epsilon = 1 - \left[\left(\frac{R_s}{R} - 1 \right) \left(1 + \frac{8}{3} \frac{\delta^2}{l^2} \right) + 1 \right]^{-3} \tag{61}$$

where the dimensionless R is equal to one. This new porosity can be substituted to the limiting trajectory equation when the model is simulated under the surge flow conditions. The new collection efficiency will be found by the simulation.

Equation (51) shows that the momentum change increases as the surge flow magnitude increases, and the porosity increases also. Consequently, the collection efficiency of the filter is decreased.

Simulation Results and Discussions

Simulation Results

The model is first simulated under the conditions of the steady input flow, and then the new porosity under the dynamic input flow will replace the original porosity of the model. To solve the first order Equation (42) is a little

bit complicated. There are at least four parameters that will influence the solution of this equation, and the correction factors of each force from Equations (24) to (33) also will be changed by moving along each point in the limiting trajectory. A numerical method of the fourth order Runge-Kutta will be introduced to simulate the solution for Equation (42) [47]. The angle θ_e of the first point which the particle enters the unit cell is the final solution of the Equation (42), so the calculation is to move the point backward through time from the last point that the particle will be captured by the collector, which is $\theta_{p0} = \pi$, $\underline{r}_{p0} = 1$. If the angle which the particle enters the unit cell is larger than the θ_e, the particle will escape from the unit cell.

As mentioned previously, there are several governing parameters that will interfere with each other when simulating the model. Therefore, it is difficult to consider and calculate them simultaneously when they change value in the simulation. To simplify the problems, the best way is to select one parameter each time and let the rest of the parameters be constant, and then the solution to the differential equation is straight forward. The results and the effects of selecting the governing parameters such as porosity ϵ , A, particle size $\underline{a}$, and the number of fiber layer N are shown in Figures 10 to 16, and the data is presented in Table I to III. The relation between these

TABLE I

RESULTS OF SIMULATION IN $\epsilon = 0.2$

a (μ m)	N = 10 (%)	N = 20	N = 30
3.0	7.1	13.7	19.8
4.5	19.0	33.0	44.0
6.0	32.2	54.0	69.0
7.5	43.8	68.4	82.2
9.0	53.2	78.1	89.8
10.5	59.5	84.1	93.6
12.0	63.3	86.5	95.1

TABLE II

RESULTS OF SIMULATION $\epsilon = 0.4$

a (μ m)	N = 10 (%)	N = 20	N = 30
3.0	0.8	1.6	2.5
4.5	1.7	2.7	4.8
6.0	2.5	4.9	7.3
7.5	13.5	25.2	35.3
9.0	19.6	35.3	47.9
10.5	25.4	44.4	58.5
12.0	31.0	52.3	67.1
13.5	36.1	59.2	74.0
15.0	40.9	65.0	79.0
16.5	45.1	69.9	83.0
18.0	48.9	73.9	86.6
19.5	52.2	77.2	89.1
21.0	55.1	79.9	91.0
22.5	57.5	82.0	92.3
24.0	59.2	83.3	93.1
25.5	60.9	84.6	94.0
27.0	62.6	86.0	94.8
28.5	63.3	86.5	95.1

TABLE III

RESULTS OF SIMULATION ϵ = 0.6

a (μ m)	N = 10 (%)	N = 20	N = 30
3.0	1.2	2.5	3.7
4.5	2.2	4.6	6.6
6.0	3.3	6.6	9.7
7.5	3.7	7.3	10.7
9.0	6.1	12.0	18.0
10.5	9.4	17.2	25.1
12.0	12.1	22.9	32.3
13.5	17.5	31.9	43.9
15.0	21.4	38.2	51.4
16.5	25.0	43.7	57.7
18.0	28.3	48.5	63.1
19.5	31.4	52.9	67.7
21.0	34.3	56.9	71.7
22.5	37.1	60.4	75.1
24.0	39.0	63.4	77.6
25.5	41.0	66.2	80.1
27.0	44.0	69.2	82.9
28.5	47.1	71.5	84.8
30.0	48.6	73.6	86.4
31.5	50.4	75.4	87.8
33.0	52.1	77.1	89.0
34.5	53.6	78.5	90.0
36.0	55.0	79.7	90.8
37.5	56.0	80.1	91.4
39.0	57.1	81.1	92.0
40.5	58.4	82.7	92.8
42.0	59.3	83.4	93.2
43.5	60.0	84.1	93.6
45.0	60.8	84.6	93.9
46.5	61.4	85.1	94.2
48.0	61.9	85.5	94.5
49.5	62.3	85.8	94.6
51.0	62.7	86.1	94.8
52.5	63.1	86.4	95.0

governing parameters and total filter efficiency will be discussed in the next section.

Discussions

To recall Equation (42), there are several governing parameters that can influence the results. Therefore, there is no single figure which can adequately represent the filtration behavior as in simulation. Basically, each figure merely shows two variable governing parameters and lets the rest of the governing parameters be constant. The detailed discussions and the figures below will show the effects of these governing parameters:

1. The porosity of the filter ϵ :

   Figures 10 to 12 show that the filtration efficiency is better when the porosity is getting smaller. It is easy to make sense that if the filter becomes more densely packed or smaller in the pore size of the filter, the smaller particles in the fluid are difficult to pass through the filter. In Figures 10 to 12, the test value of ϵ is 0.4 and 0.6, A = 1 10^{10}, and N = 10, 20, 30 sequential in Figures 10 to 12.

2. The number of fiber layers N in the filter:

   The effect of the number of fiber layer N are shown as Figures 13 to 15. The more numbers of the fiber layers are in the filter, and the better the total efficiency of the filter is. Since more layers are

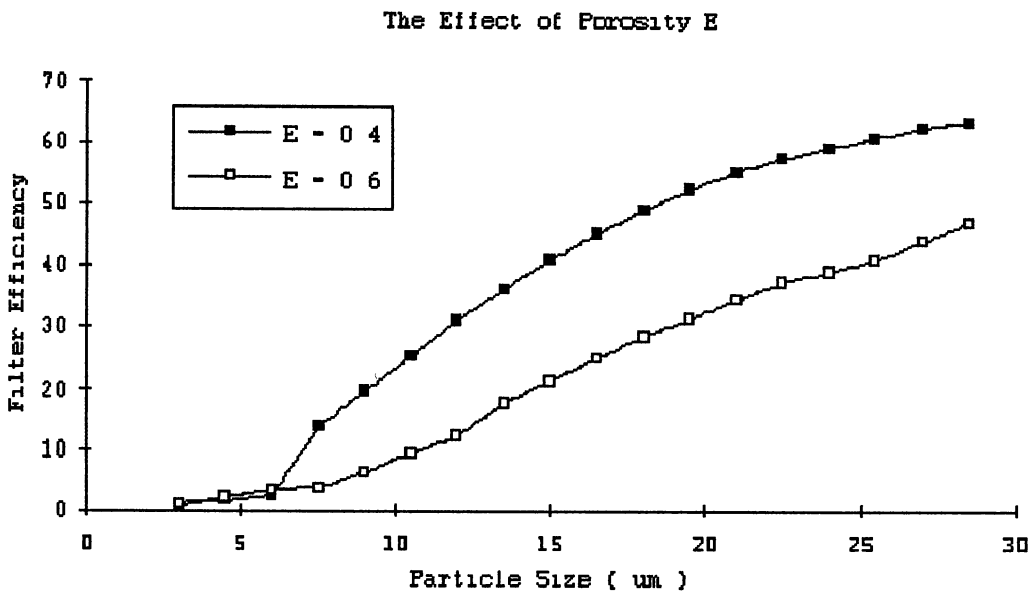

Figure 10. The Effect of Porosity (N = 10)

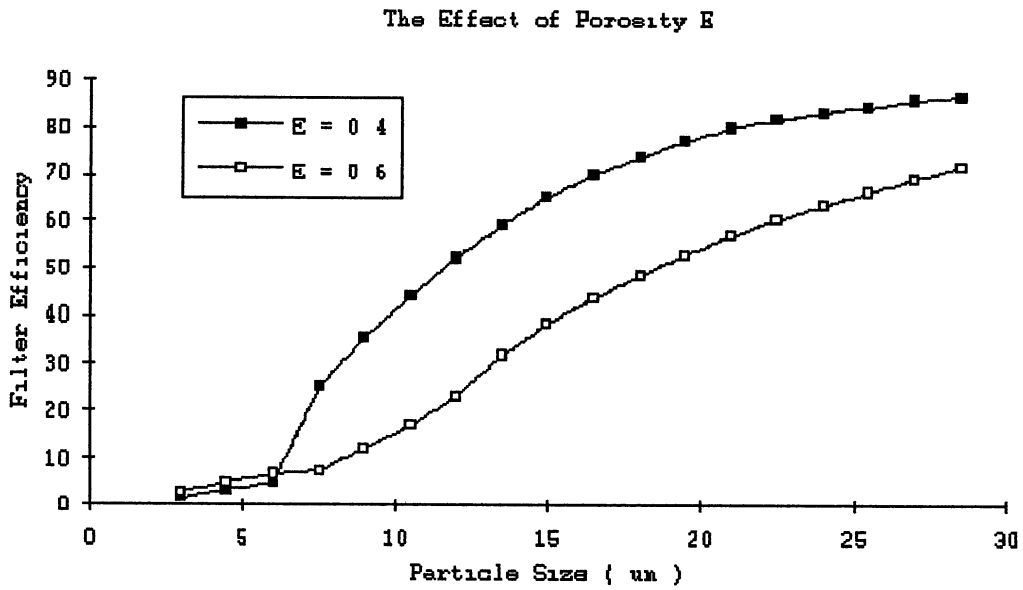

Figure 11. The Effect of Porosity (N = 20)

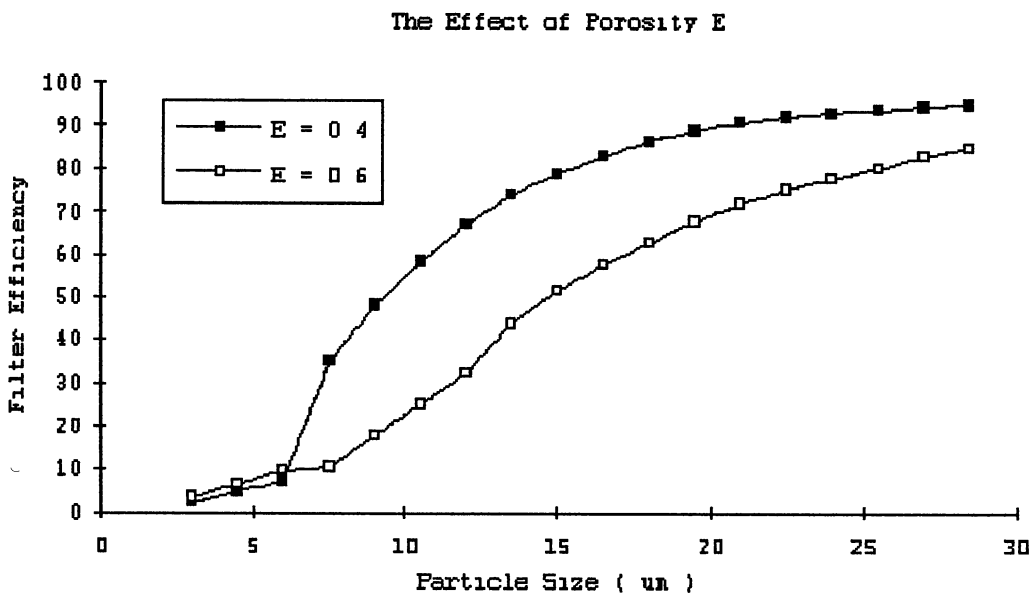

Figure 12. The Effect of Porosity (N = 30)

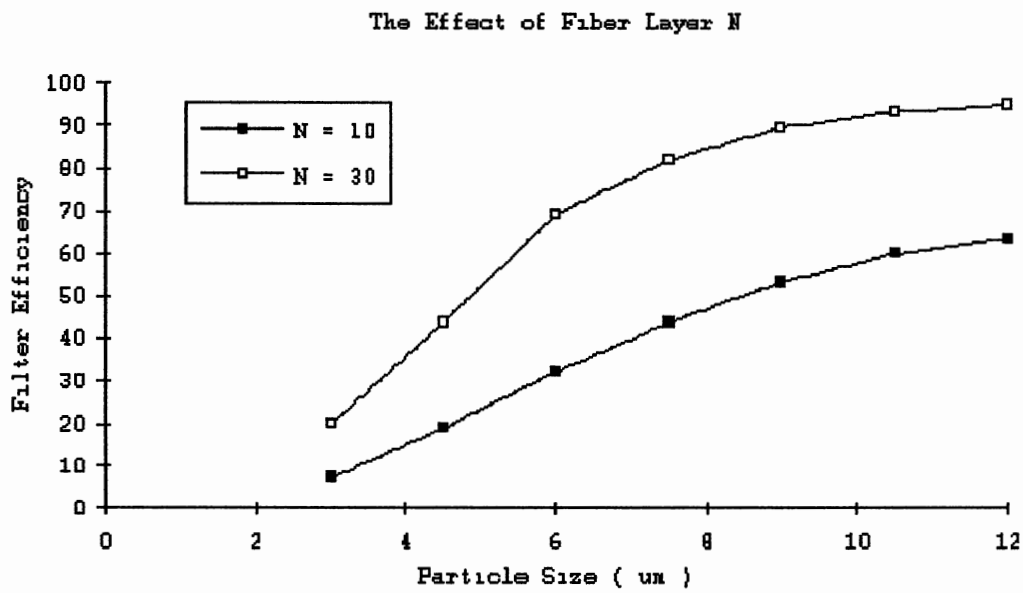

Figure 13. The Effect of Fiber Layer (ϵ = 0.2)

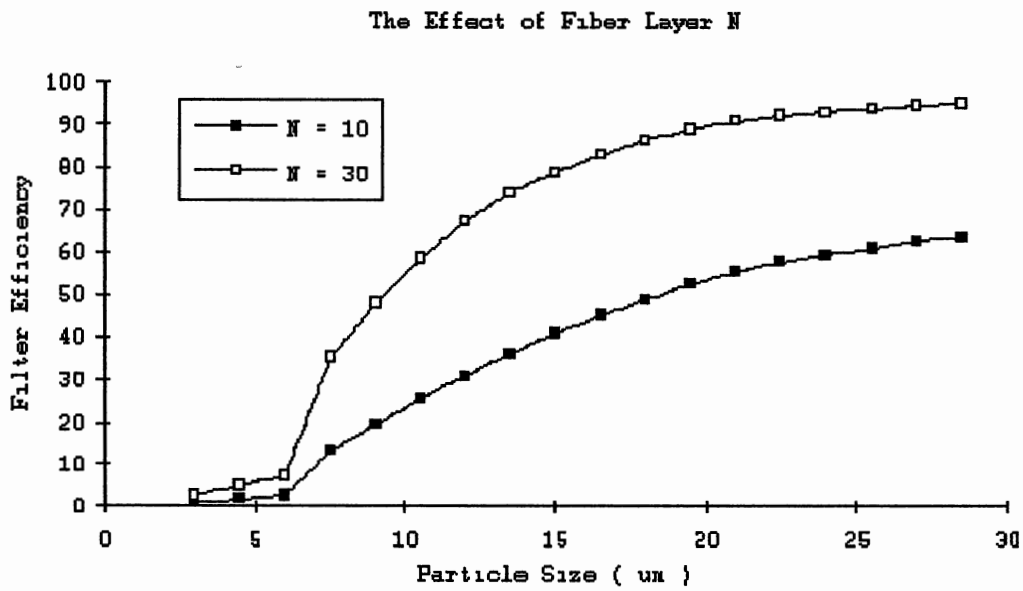

Figure 14. The Effect of Fiber Layer (ϵ = 0.4)

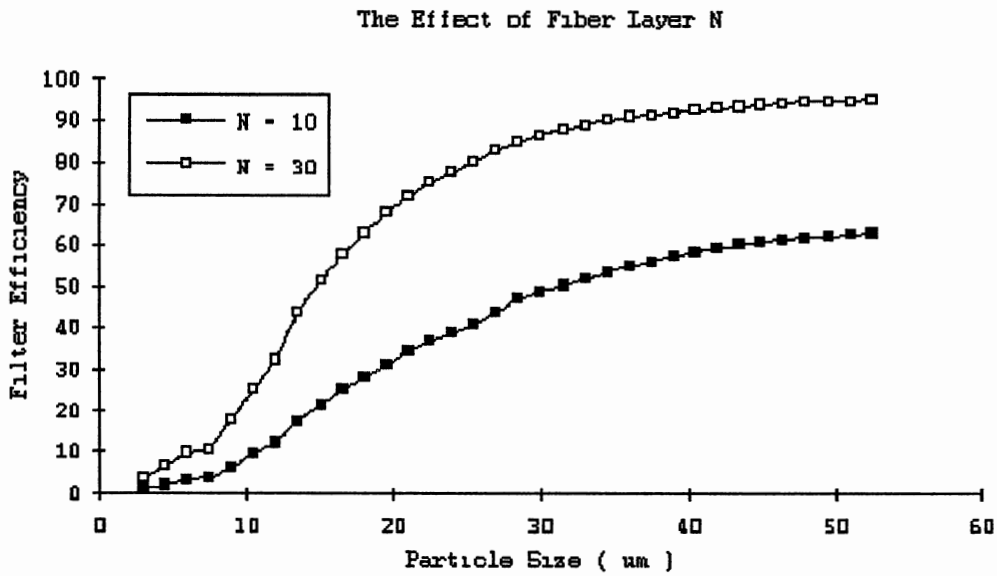

Figure 15. The Effect of Fiber Layer (ϵ = 0.6)

in the filter, the probability of the particles that are captured by the filter becomes higher. The reason is that the pore size distribution is changed and the diameter of the pore gets smaller. Therefore, the larger particles will be trapped by the filter easily [48, 49]. The test value of N is 10 and 30, A = 1 10^{10}, and ϵ is 0.2, 0.4, 0.6 sequential in Figures 13 to 15.

3. The value of A:

The parameter A is the ratio of fluid viscous forces to Van Der Waals forces, and it is effective only when the particle is very near the collector. At this time, the Van Der Waals forces are large enough to overcome the fluid viscous forces and attract the particles to be captured on the surface of the unit cell. Therefore, if the particle is at a distance from the unit cell, this ratio A will be a big amount to the unit cell when A compares with others' parameters. Generally, the range of the A is from 10^9 to 10^{12}, which is reasonable for actual filters and lubricants. In Figure 16 the different values of the A are substituted to Equation (42), but these different values do not change the shape of the curve. The main reason is that the A is in the denominator of Equation (42), so the inverse value of the A is very small that can not influence the results. Figure 16 will show the A in 10^{10} and 10^{12}

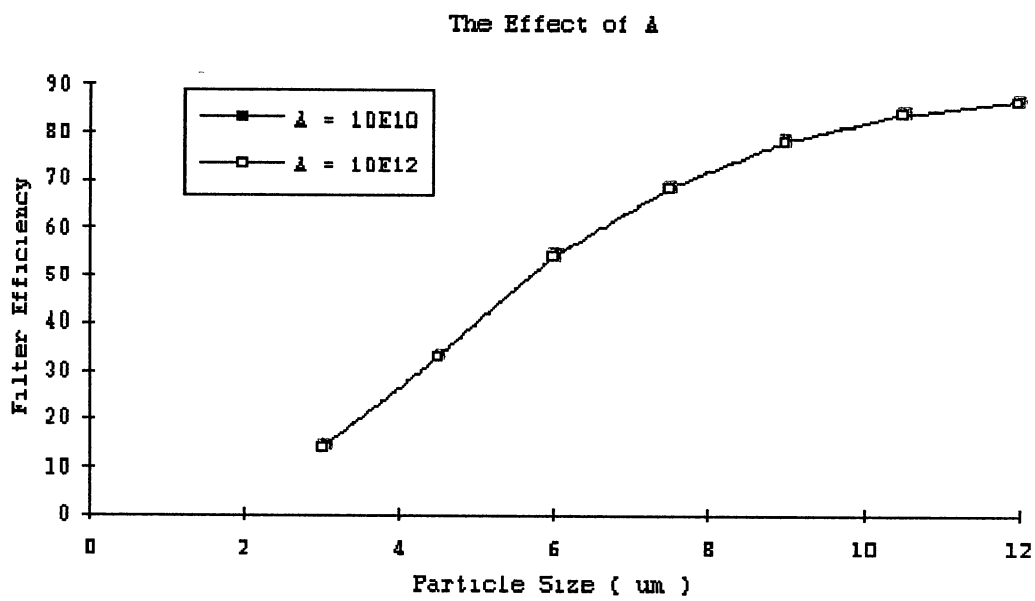

Figure 16. The Effect of A (N = 20, ϵ = 0.2)

when the porosity ϵ is 0.4 and N is 30.

4. The effects of forces and torques:

   When the particle is very close to the collector, the forces and torques from a moving particle in a stationary fluid will be very large, especially the $\underline{F}_r^n$ is very important in Equation (42). Generally speaking, no special force and torque items will change the result of Equation (42) significantly.

In the next chapter, the experimental results are presented to verify the results from the simulation of the theoretical model.

CHAPTER IV

EXPERIMENTAL VERIFICATION OF THE FILTER MODEL UNDER DYNAMIC FLOW

Introduction

The performance of the contamination levels in the fluid power system always encounters the filter under the dynamic operating conditions. The knowledge required to evaluate the collection efficiency under steady flow operating conditions is more simple than under dynamic flow operation. Tests are available which evaluate the filtration process and the performance of the filter efficiency under steady flow input, but the results usually can not be applied directly to the actual field system. The main reason is that the results of the tests are obtained with constant parameters. In field operation these system parameters are not constant. Therefore, steady flow test results must be applied very carefully.

Cyclic flow tests have been carried out to determine the effects under dynamic flow. The test of Bensch [38] has proven that filter efficiency decreased under dynamic flow input. Moreover, in test presented by Gehrking [37] the same trend was revealed.

Test Method

The test method used by Bensch for conducting cyclic flow tests was intended to simulate the multi-pass test procedure with continually varying flow rate. To simulate the filter under the surge flow input, the model will use the cyclic flow to represent the flow rate. A simple modification of the test has been made in the by-pass line which permits the generation of the cyclic flow through the filter. Figure 17 presents the standard multi-pass test circuit.

A variable-low speed motor is fixed to a ball valve and is inserted in the by-pass line. Figure 18 shows this motorized ball valve. When the ball valve is fully open, no flow will pass through the filter. If it is closed, rated flow will be subjected to the filter. An ideal flow rate is assumed to vary in a nearly sinusoidal manner. This uniform flow rate can be formulated as

$$Q_f = M + P\sin(2\pi ft) \tag{62}$$

where

M : average flow rate

P : magnitude of oscillation

f : frequency of oscillation

Equation (62) can be plotted as Figure 19.

The hydraulic system set up for the cyclic flow test is very similar to the basic multi-pass test. The difference

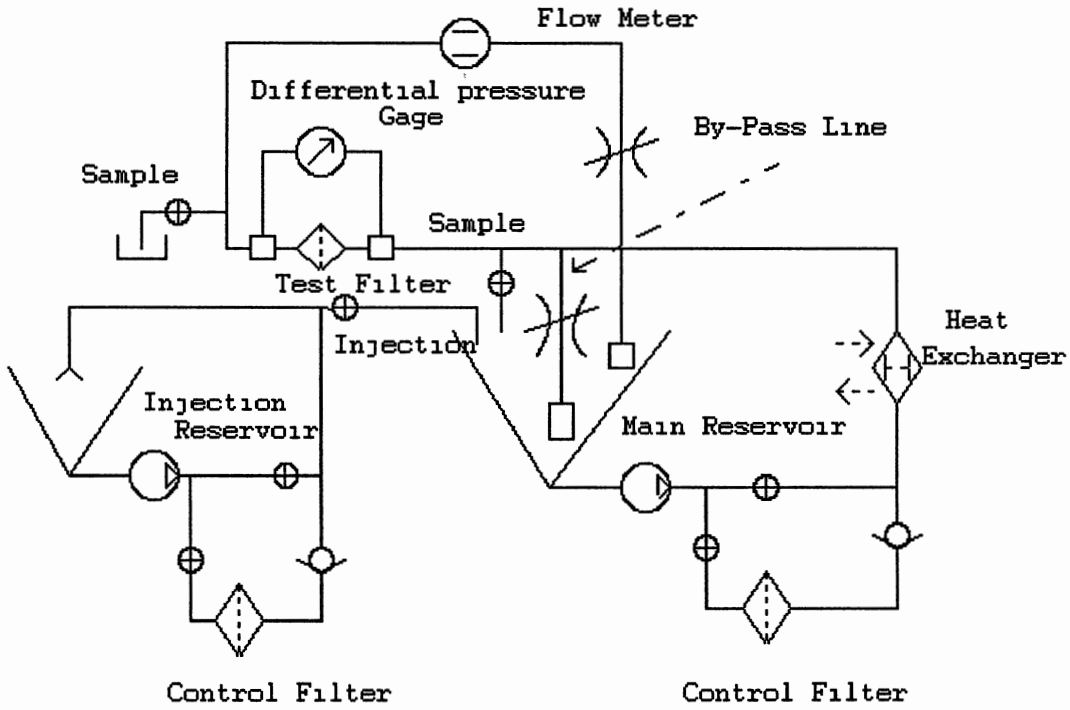

Figure 17. Schematic of Multi-pass Filter Test Circuit

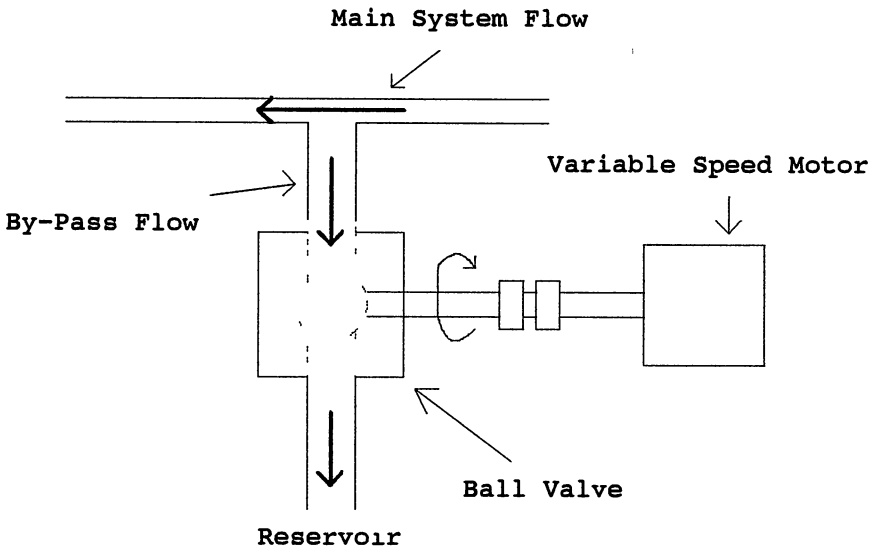

Figure 18. Motorized Ball Valve

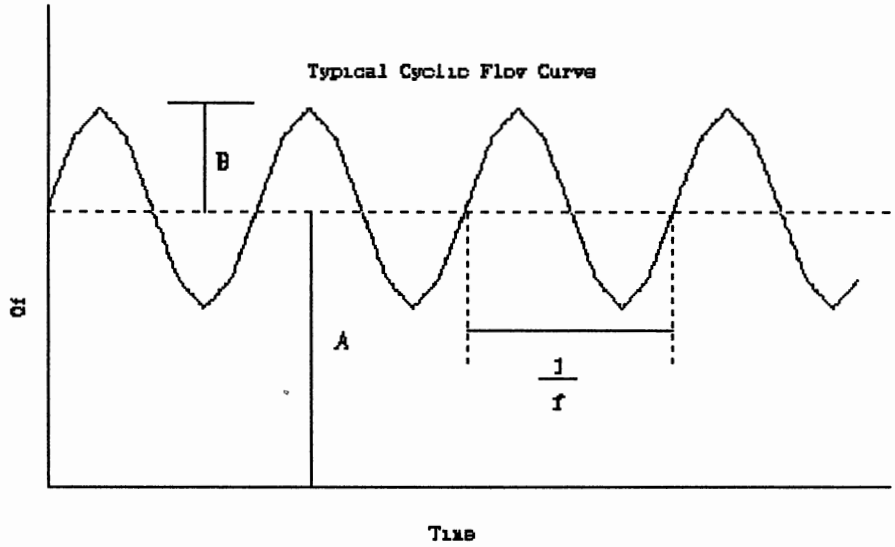

Figure 19. Typical Cyclic Flow Curve

between these two tests depends on whether the motorized ball valve is installed in the test or not.

Test Facility

The test facility used to operate a multi-pass filter test is shown in Figure 17. The test facility consists of two separate systems. One is a filter test system, and the other is a contamination injection system. Both of these systems contain heat exchanger, cleanup filter loop, return line flow diffusers, contaminant insensitive pump, and reservoirs which have the conical bottom [2]. These two systems will discharge the fluid to the reservoir of the main filter test system. The fluid flow is divided into several branches, and a portion of the flow in the filter test system passes through the test filter directly. Afterwards, this portion of flow is through the flow meter before this flow discharges into the system reservoir.

The test system is qualified by the ISO standard. This qualification will maintain the contaminant in suspension under the lowest flow rate and let test be going as long as expected. Moreover, the circulation system must retain particles in suspension and prevent them from being destroyed.

Test Procedure

In a standard multi-pass filtration performance test, the test filter is subjected to a constant flow, and

contaminant is injected to this filter continuously until the pressure differential across the test filter increase by a specified amount.

When the by-pass valve is fully closed, a rated flow will be subjected to the test filter, and the initial value of the pressure difference is obtained. The cyclic flow is initialed along with the injection flow. A strip recorder that was used to across the test filter monitored and recorded the flow cycle and pressure differential continuously. The samples from the contaminant flow were taken when the pressure drop reaches the 10%, 20%, 30%, 40%, and 80% of the final pressure drop. The particles were count in the samples of both upstream and downstream. The particle count data was used to determine the β_{10} ratio of the test filter. The Beta ratio, at a given size, is defined as the cumulative number of particles greater than the given size upstream divided by the number of particles greater than the same size downstream of the filter [36].

In a second test series reported by Bensch [39], different magnitudes of flow surges in the test system (based on the multi-pass test method described above) were obtained by using three by-pass ball valves installed in a parallel arrangement in the system by-pass line. Each by-pass ball valve diverted a different amount of flow around the test filter. When these ball valves are opened and closed quickly, different magnitude flow will be subjected to the filter.

Result of Cyclic Test

The test results reported by Bensch [39] using different surge magnitudes are shown in Table IV and Figure 20, which illustrate the reduction in the 10 micrometer filtration ratio that occurs when the different magnitude surge flows are subjected to different test filters. When the flow magnitude is increased, each test filter exhibits a general Beta reduction. In fact, most of them have a filtration ratio less than 20% of the original steady flow values, as high surge flow are subjected to these test filters.

Similar results are shown in Figure 21 based on data presented by Gehrking [37]. The collection efficiency of the test filter is significantly decreased with the surge flow. In addition, a similar test carried out during this research that uses an on-off machine to replace the motorized ball valve is presented in Figure 22. The test results have the same trends as those reported by Bensch [39] and Gehrking [37].

Discussion of Results

In order to obtain results from the cyclic flow filter model, it was necessary to assume mat length, mat thickness, mat porosity, material bulk modules, etc. Most of these parameters can not be accurately measured on actual filter elements such as were used in the experimental tests.

TABLE IV

RESULTS OF SURGE FLOW TEST

Filter		1	2
Surge #1	Surge Magnitude[1]	1.23	1.24
	β_{10} Before	4.80	28.50
	β_{10} After	7.30	25.30
	β_{10} Reduction[2]	1.52	0.89
Surge #2	Surge Magnitude	1.80	1.81
	β_{10} Before	6.60	35.10
	β_{10} After	6.70	27.20
	β_{10} Reduction	1.01	0.77
Surge #3	Surge Magnitude	1.90	1.88
	β_{10} Before	5.20	16.20
	β_{10} After	6.60	6.01
	β_{10} Reduction	1.27	0.37
Surge #4	Surge Magnitude	2.55	2.50
	β_{10} Before	8.40	76.00
	β_{10} After	4.00	9.33
	β_{10} Reduction	0.48	0.12
Surge #5	Surge Magnitude	2.78	2.70
	β_{10} Before	9.10	21.50
	β_{10} After	2.09	2.62
	β_{10} Reduction	0.23	0.12

1. Surge magnitude is the ratio of the flow rate after the surge to that before.
2. β_{10} reduction is the ratio of β_{10} after the surge to that before the surge.

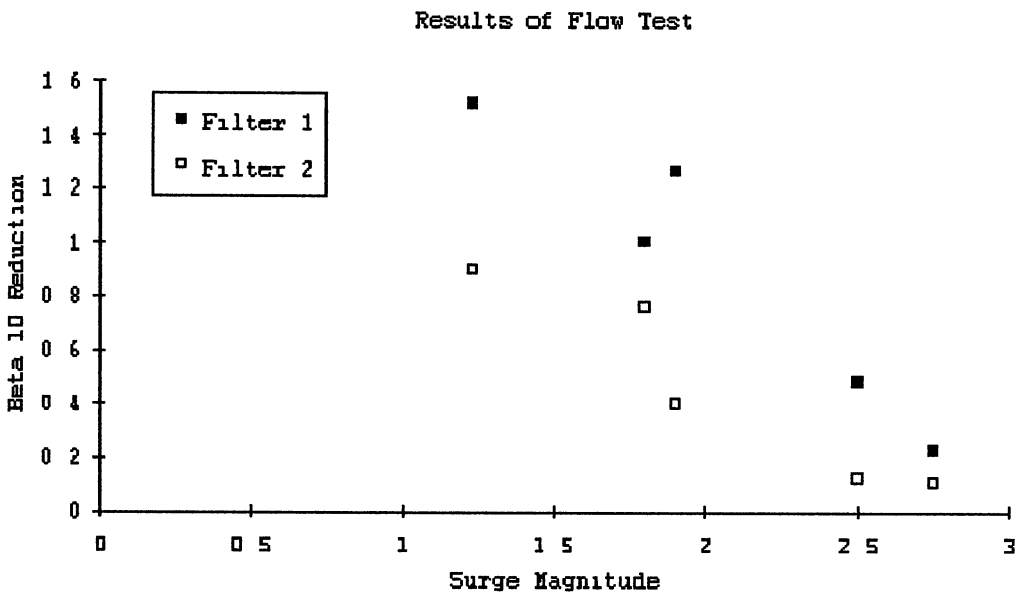

Figure 20. Surge Flow Test Results

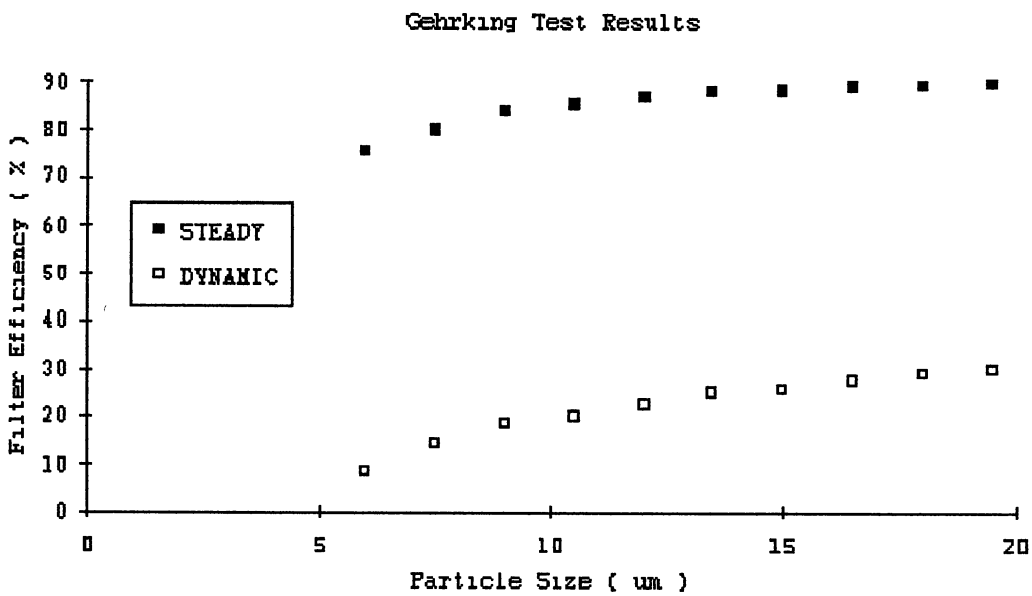

Figure 21. Test Results (Gehrking [37])

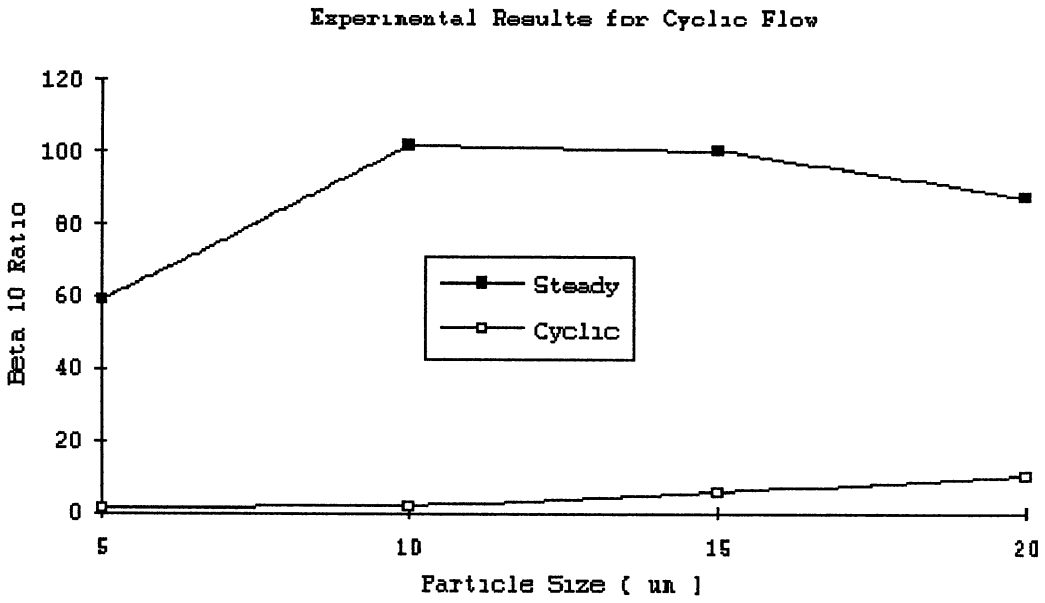

Figure 22. Experimental Results for Dynamic Flow

Therefore, a comparison between the model results and the experimental results must be done on a trend based.

In comparison with Bensch results, the following data were used in the calculation.

data obtained form actual filter:

l = 1.905 cm

h = 1.5 10^{-2} cm

assumed data:

ϵ = 0.4

E = 2 10^{6} psi

ν = 0.3

q1 = 5 psi (pressure induced by a surge flow of 0 to 30 gpm)

q2 = 10 psi (pressure induced by a surge flow of 0 to 60 gpm)

The simulation results are shown in Figure 23 and Table V. For comparison purpose, if a specific particle size, e.g. 15 micrometer, is selected from Figure 23, the relation between efficiency reduction of that size and the applied flow magnitude can be obtained. This relation is presented in Figure 24. Note that the trend of the filter efficiency reduction obtained from simulation is similar to Bensch's test data. Further, Table VI and Figure 25 shows a good correlation in trends between the simulation and Gehrking's test data.

TABLE V

SIMULATION RESULTS OF SURGE FLOW TEST

Simulation Results			Bensch Test Results		
Magnitude	N = 10	N = 30	Magnitude	Filter 1	Filter 2
0.0	1.0	1.0	1.23	1.09	0.998
1.0	0.961[1]	0.984	1.80	1.0	0.991
2.0	0.778	0.865	1.90	1.05	0.888
			2.55	0.851	0.904
			2.78	0.585	0.641

1. Filter Efficiency Reduction

TABLE VI

SIMULATION RESULTS OF DYNAMIC FLOW TEST

Particle Size (μ m)	Simulation Results Const. %	Simulation Results Dynam. %	Gehrking Test Results Const. %	Gehrking Test Results Dynam. %
7.5	35.3	24.0	80.0	14.3
9.0	47.9	34.3	84.1	18.5
10.5	58.5	45.2	85.7	20.1
12.0	67.1	54.3	87.0	22.7
13.5	74.0	61.9	88.1	25.3
15.0	79.0	68.3	88.3	26.1
16.5	83.0	73.6	89.2	27.9
18.0	86.6	78.0	89.6	29.4
19.5	89.1	82.1	89.8	29.8

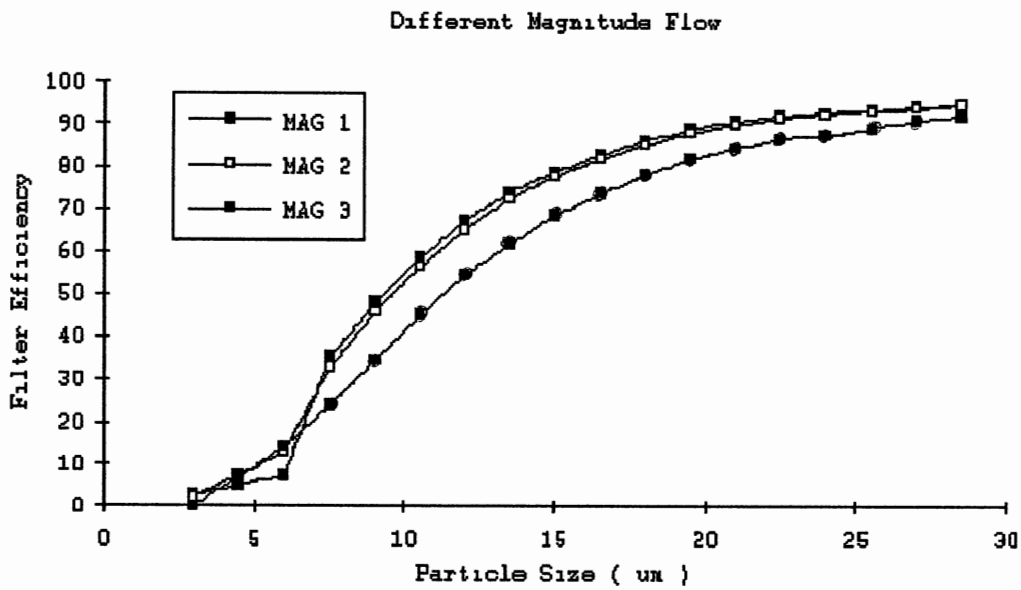

$N = 30$, $A = 1 \cdot 10^{10}$
Magnitude 1: $\epsilon = 0.4$
Magnitude 2: $\epsilon = 0.413$
Magnitude 3: $\epsilon = 0.478$

Figure 23. Different Magnitude Flow

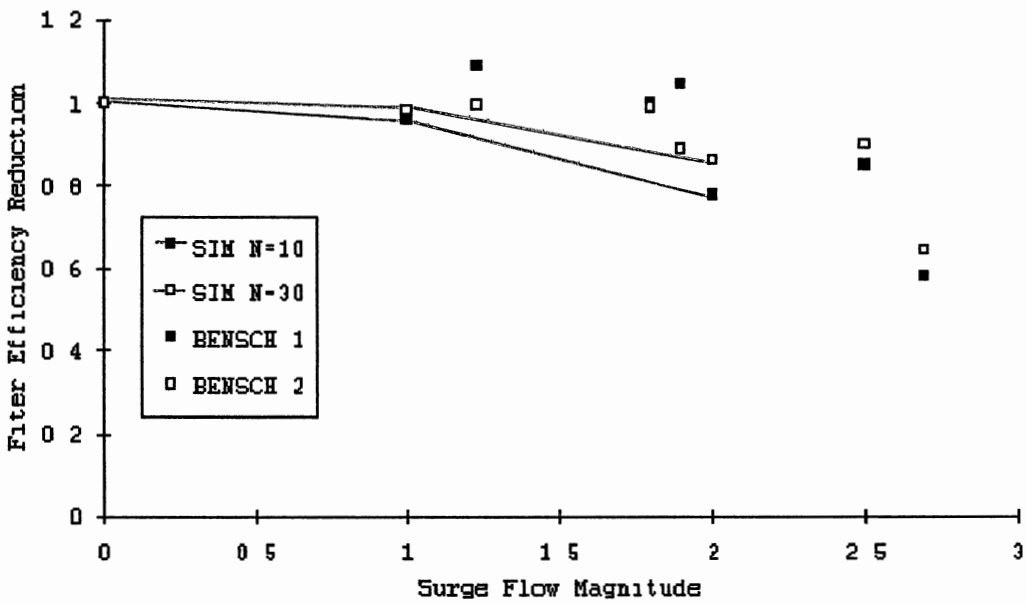

$A = 1 \cdot 10^{10}$
Particle Size = 15 μ m

Figure 24. Comparison of Dynamic Flow Test Data 1 with Simulation Results

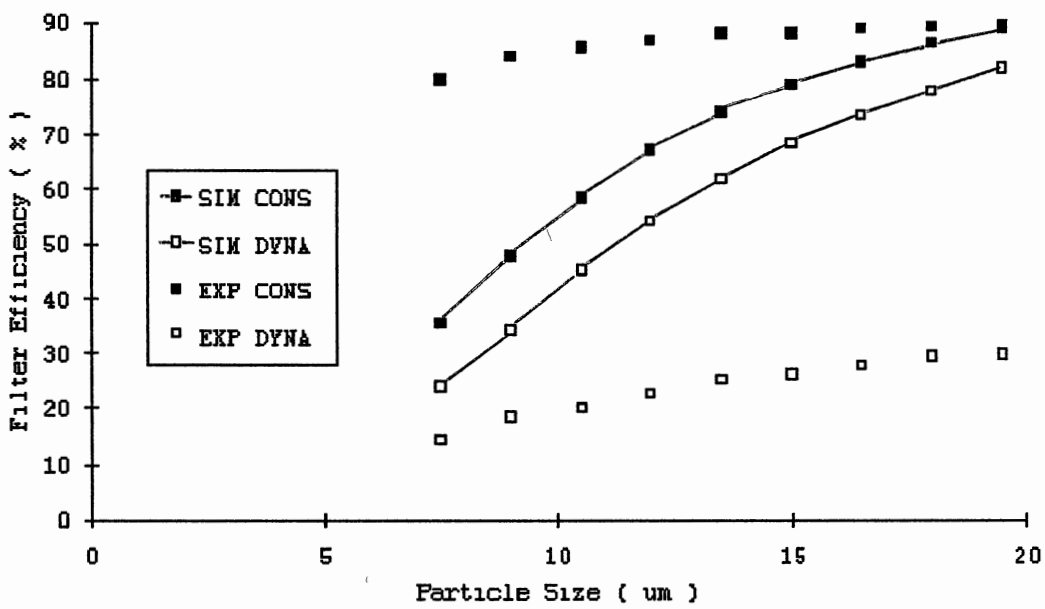

$N = 30$, $A = 1 \cdot 10^{10}$
Constant flow: $\epsilon = 0.4$
Dynamic flow: $\epsilon = 0.478$

Figure 25. Comparison of Dynamic Flow Test 2 with Simulation Results

CHAPTER V

CONCLUSIONS AND RECOMMENDATION

Conclusions

This thesis studies into the problems of particle retention characteristics in an interstitial regime under dynamic flow conditions. The overall objective was to develop a theoretical filter model, based on particle retention characteristics that can predict the performance of a filter not only under the steady flow, but also under the dynamic flow input.

A filter is very important to hydraulic systems. If there are too many unwanted particles in the fluid, they will reduce the efficiency and life of the hydraulic system. Although a filter is used to remove the particles from the lubricants, there is no filter that can stop all the particles in the lubricants completely. To reduced the cost of maintenance, it is necessary to have a suitable filter to protect the system from harmful contaminant particles.

Today, theoretical models only consider filter characteristics under steady flow conditions. The basic informations from these models are necessary in designing and selecting filters. However, most hydraulic filters, especially those which are installed in the return lines of

hydraulic systems, seldom operate under steady flow conditions. The unability to analytically evaluate filter efficiency in practical situation is a serious deficiency in filtration technology.

In this research, the approach is based on modeling the filter as a uniformly distributed fiber mat which includes many unit cells. The particles suspended in the fluid are assumed to follow the limiting trajectory in their approach to the collectors of the unit cell. Several forces are considered in the model, especially the Van Der Waals forces and fluid viscous forces. When the Van Der Waals force between particle and the collector overcomes the fluid viscous force, the particle will collide with the collector.

The collection efficiency was obtained by solving the limiting trajectory equation which is a function of the viscous number A, the relative particle size a, the number of the fiber layer N, and the porosity e of the fiber mat. These critical parameters influence the simulation results. The effects of these parameters are shown in the relevant figures in the preceding chapters.

To predict the performance of a filter under the dynamic operating conditions, the associated porosity of the fiber mat was obtained based upon the momentum change caused by the surge flow. The model shows that when the surge flow magnitude is increased, the porosity of the filter will also increase. Furthermore, the model reveals that this porosity increase will reduce the collection efficiency.

Surge flow tests have been conducted to determine the effects of the filter under dynamic state. In all of those tests, the results shown that the filtration ratio is decreased by increasing the magnitude of the surge flow which was validated by the model developed here, and a high correlation in trends was obtained. These findings illustrate that the contamination level in a hydraulic system under dynamic operating conditions will always be higher than that found by conducting the filter tests under the steady flow conditions.

In summary, the research reported here has developed an analytical model for filter performance under dynamic flow operation. This model was verified using actual filter test data. The use of this model can provide a system designer a tool to qualitatively predict the trends of filter efficiency under dynamic situation.

Recommendations

While the filters are successfully used in hydraulic application, filtration technology does not provide sufficient predictive capability. This research explores the theoretical characteristics of filtration processes under variable flow conditions. It offers valuable technical knowledge regarding the properties of particle mechanisms and forces acting on the filter. In order to promote the development of the technology to complete the

study of filter performance, the following is a list of suggestions which can provide for advanced research:

1. The fiber distribution is assumed to be uniformly distributed in the filter model but, in the actual hydraulic filter, this kind of distribution may be difficult to find. The normal distribution is widely used to represent the pore size of the filter mat. Therefore, in future studies it is possible to replace uniform distribution to normal or log-normal distribution of the pore size in the model.
2. Pressure drop is an important parameter to be considered. When the particles of contaminants clog the pores of the fiber mat, the pressure drop of the filter will increase. Under this circumstance, the particle will be forced to pass through the pore of the filter.
3. In this study it was assumed that if the particle is captured, it never escapes from the collector. In the actual system, mechanical disturbance due to the system vibration may dislodge the capture particle. Therefore, the influence of system vibration should be investigated.
4. Thermal properties may change due to temperature of filter mat and contaminant particles. The thermal effects on pore size distribution should be considered.

BIBLIOGRAPHY

1. Rosenfeld, L. "The Removal of Contaminant from Automotive Lubricating Oil -- Problems and Prospects." Filtration and Separation, (1969), 150-154.

2. Fitch, E. C. An Encyclopedia of Fluid Contamination Control. Washington, D. C. : Hemisphere Publishing Co., 1980.

3. Wong, J. B., Ranz, W. E. and Johnstone, H. F. "Collection Efficiency of Aerosol Particles and Resistance to Flow Through Fiber Mats." Journal of Applied Physics, 27 (1956), 161-169.

4. Bensch, L. E. "Transport and Retention Mechanisms." Basic Fluid Power Research Program, Oklahoma State University, No. 71-3, Stillwater, Oklahoma, (1971).

5. Rajagopalan, R. Stochastic Modeling and Experimental Analysis of Particle Transport in Water Filtration. Ph.D. Dissertation, Syracuse University, 1974.

6. Spielman, L. A. "Particle Capture from Low-Speed Laminar Flows." Ann. Rev. Fluid Mech., 9 (1977), 297-319.

7. Spielman, L. A. and FitzPatrick, J. A. "Theory for Particle Collection under London and Gravity Forces." Journal of Colloid and Interface Science, 42 (1973), 607-623.

8. Kitzmiller, D. and Bensch, L. E. "Fundamental Properties of Test Contaminants." Fluid Power Research Conference, Oklahoma State University, No. P75-8, Stillwater, Oklahoma, (1975).

9. Kinsley, H. B. "The Relationship Between Fiber Diameter and Filtration Efficiency." Tappi, 72 (1989), 153-156.

10. Bensch, L. E. and Tessmann, R. K. "Particle Counting Statistics." Basic Fluid Power Research Program, Oklahoma State University, No. 75-11, Stillwater, Oklahoma, (1975).

11. Fitch, E. C. "The Multipass Filter Test -- Now a Variable Tool." Basic Fluid Power Research Program, Oklahoma State University, No. 74-39, Stillwater, Oklahoma, (1974).

12. Happel, J. "Viscous Flow in Multiparticle System: Slow Motion of Fluids Relative to Beds of Spherical Particles." AIChE Journal, 4 (1958), 197-201.

13. Payatakes, A. C., Rajagopalan, R. and Tien, C. "On the Use of Happel's Model for Filtration Studies." Journal of Colloid and Interface Science, 49 (1974), 321-325.

14. Spielman, L. A. and FitzPatrick, J. A. "On the Use of Happel's Model for Filtration Studies-Note in Reply." Journal of Colloid and Interface Science, 49 (1974), 328-329.

15. Happel, J. and Bernner, H. Low Reynolds Number Hydrodynamics, Prentice Hall, Englewood Cliffs, New Jersey, 1965.

16. Yao, K. M. Influence of Suspended Particle Size on the Transport Aspect of Water Filtration. Ph.D. Dissertation, University of North Carolina, 1968.

17. Yao, K. M., Habibian, M. T. and O'Media C. R. "Water and Waste Filtration: Conceptions and Applications." Environmental Science & Technology, 5 (1971), 1105-1112.

18. Corte, H. K. and Lloyd, E. H. "Fluid Flow Through Paper and Sheet Structure." Consolidation of the Paper Web, Ed. F. Bolam (Technical Section, B.P. & B.M.A., London), 1966.

19. Carman, P. C. "Fluid Flow Through Granular Beds." Transactions--Institution of Chemical Engineers. (1937), 150-166.

20. "Pore Size Distribution and Pressure Drop Models in Fibrous Filter Media." Basic Fluid Power Research Program, Oklahoma State University, No. 71-3, Stillwater, Oklahoma, (1971).

21. Cranston, R. W. "Filtration of Aerosols by Fiber Media." Chem. Revs., 55 (1955), 595-623.

22. Werner, R. M. and Clarenburg, L. A. "Aerosol Filters--Pressure Drop across Single-Component Glass Fiber Filters." I&EC Process Design and Development, 4 (1965), 288-293.

23. Johnson, P. R. "Fluid Filter Media: Measuring the Average Pore Size and the Pore-Size Distribution, and Correlation with Results of Filtration Tests." Journal of Testing and Evaluation, (1985), 308-315.

24. FitzPatrick, J. A. Mechanisms of Particle Capture in Water Filtration, Ph.D. Dissertation, Havard University, 1972.

25. Rajagopalan, R. and Tien, C. "Trajectory Analysis of Deep-Bed Filtration with the Sphere-in-cell Porous Media Model." AIChE Journal, 22 (1976), 523-533.

26. Tichy, J. A. "A Model for Optimum filtration of a Lubrication." Wear, 111 (1986), 73-82.

27. Tichy, J. A. "A Model of Lubrication Filtration." Journal of Lubrication Technology, 103 (1981), 81-89.

28. Fitchman, M. and Pnueli, D. "Sufficien Condition for Small Particle to Hold Together Because of Adhesion Forces." Journal of Applied Mechanics, 52 (1985), 105-108.

29. Hamaker, H. C. "The London-Van Der Waals Attraction Between Spherical Particles." Physica IV, 23 (1937), 1058-1072.

30. Goldman, A. J., Cox, R. G. and Bernner, H. "The Slow Motion of Two Identical Arbitrarily Oriented Spheres Through a Viscous Fluid." Chemical Engineering Science, 21 (1966), 1151-1170.

31. Goldman, A. J., Cox, R. G. and Bernner, H. "Slow Viscous Motion of a Sphere Parallel to a Plane Wall-I. Motion Through a Quiescent Fluid." Chemical Engineering Science, 22 (1967), 637-651.

32. Bernner, H. "The Slow Motion of a Sphere Through a Viscous Fluid Towards a Plane Surface." Chemical Engineering Science, 16 (1961), 242-251.

33. O'Nell M. E. "A Slow Motion of Viscous Liquid Caused by a Slowly Moving Solid Sphere." Mathematika, 11 (1964), 67-73.

34. Goren, S. L. "The Normal Force Exerted by Creeping Flow on a Small Sphere Touching a Plane." Journal of Fluid Mech., 41 (1970), 619-625.

35. Goren, S. L. and O'Nell M. E. "On the Hydrodynamic Resistance to a Particle of a Dilute Suspension When

in the Neighborhood of a Large Obstacle." Chemical Engineering Science, 26 (1971), 325-338.

36. Pierce, J. D. "Filter Performance with Cyclic Flow." SAE Technical Paper Series, No. 860736, 1986.

37. Gehrking, J. N. "Measurement of Hydraulic Filter Performance During Cyclic Flow." 37th Annual Meeting, National Conference on Fluid Power, 1981.

38. Bensch, L. E. "The Influence of Surge Flow on Filter Performance." SAE Technical Paper Series, No. 86037, 1986.

39. Bensch, L. E. "Surge Flow Effects on Filter Performance." 7th Annual Fluid Power Research Conference, Oklahoma State University, No. 73-5, Stillwater, Oklahoma, 1973.

40. Bensch, L. E. "A Cyclic Flow Test for Fluid Power Filters." 8th Annual Fluid Power Research Conference, Oklahoma State University, No. 74-38, Stillwater, Oklahoma, 1974.

41. Gehrking, J. N. "Does Cyclic Flow Affect Hydraulic Filter Performance?" Hydraulic & Pneumatics, 1982.

42. Bensch, L. E. "The Influence of Surge Flow on Filter Performance." 6th Annual Fluid Power Research Conference, Oklahoma State University, Stillwater, Oklahoma, No. 72-5, 1972.

43. Hamielec, A. E., Hoffman, T. W. and Ross, L. L. "Numerical Solution of the Navier-Stokes Equation for Flow Past Spheres: Part1. Viscous Flow Around Sphere with and Without Radial Mass Efflux." AIChE, 13 (1967), 212-219.

44. Spielman, L. A. and Goren, S. L. "Capture of Small Particles by London Forces from Low-Speed Liquid Flows." Environmental Science & Technology, 4 (1970), 135-140.

45. Timoshenko, S. Strength of Materials, New York, D.Van Nostrand Company, Inc. 1940.

46. Timoshenko, S. Theory of Plates & Shells, New York, McGraw-Hill Book Company, Inc. 1959.

47. Gerald, C. F. and Wheatley, P. O. Applied Numerical Analysis, Addison Wesley, 1989.

48. Corte, H. "Pore Size Distribution of Paper." Filtration & Separation, (1966), 396-403.

49. Kallmes, O., Corte, H. and Bernier, G. :The Structure of Paper. II. The Statistical Geometry of A Multiplanar Fiber Network." Tappi, 44 (1961), 519-528.

VITA

Cheng-Sheng Ku

Candidate for the Degree of

Master of Science

Thesis. PARTICLE RETENTION CHARACTERISTICS IN AN INTERSTITIAL REGIME UNDER CYCLIC FLOW LOADING

Major Field: Mechanical Engineering

Biographical:

Personal Data Born in Taipei, Taiwan, November 25, 1962, the son of Mr W L Ku and Mrs T M Shieh.

Education Graduated from Chenkung High School, Taipei, Taiwan, in June, 1981; received the Bachelor of Science degree from National Taiwan University in June, 1986, completed requirements for the Master of Science degree at Oklahoma State University in December, 1991

Professional Experience Instructor, China Army, July, 1986, to May, 1988, Teaching Assistant, Department of Mechanical Engineering, Oklahoma State University, August, 1990, to December, 1990

Professional and Academic Affiliation: The Honor Society of Phi Kappa Phi